Quantum dynamics and control of vibrational dephasing

2004 J. Phys.: Condens. Matter 16 R1057

(http://iopscience.iop.org/0953-8984/16/30/R02)

INSTITUTE OF PHYSICS PUBLISHING JOURNAL OF PHYSICS: CONDENSED MATTER

J. Phys.: Condens. Matter **16** (2004) R1057–R1088 PII: S0953-8984(04)58970-1

TOPICAL REVIEW

Quantum dynamics and control of vibrational dephasing

Martin Gruebele

Departments of Chemistry, Physics, Center for Biophysics and Computational Biology, and Beckman Institute for Advanced Science and Technology, University of Illinois, 600 S Mathews Avenue 5-6, Urbana, IL 61801, USA

E-mail: gruebele@scs.uiuc.edu

Received 8 February 2004
Published 16 July 2004
Online at stacks.iop.org/JPhysCM/16/R1057
doi:10.1088/0953-8984/16/30/R02

Abstract

This review emphasizes the physical principles underlying the dephasing of nonstationary vibrational states of molecules with multiple vibrational degrees of freedom. The motion of atoms within molecules can be described to a very good approximation by a many-level system of coupled anharmonic quantized oscillators. The separation of electronic and nuclear timescales, combined with weak symmetry breaking inherent in molecular structures, guarantees that the Hamiltonian can always be cast in a form that is local in the quantum state space of the molecular vibrations. The resulting nonexponential dephasing dynamics can be controlled with external fields to stabilize nonstationary quantum states, and both quantum–classical and fully quantum control formalisms are described. Coupled molecular vibrations interacting with external fields also offer prospects for quantum computing because vibrational level spacings can be made very large compared to thermal noise, and relaxation mechanisms such as infrared fluorescence are many orders of magnitude slower than the timescales required for coherence transfer. Finally, a toy model that provides insights into the interaction of vibrational degrees of freedom with 'solvent' modes is also discussed, and exhibits nonexponential dynamics in certain regimes.

(Some figures in this article are in colour only in the electronic version)

Contents

1. Introduction

Optical quantum control has become an important tool in atomic, materials, and molecular physics. Examples from each of these areas include the creation of highly nonclassical atomic states [1], of solitons in optoelectronic substrates [2], and the localization of nuclear wavefunctions of diatomic molecules [3]. These processes rely on creating phase-correlated off-diagonal elements $\hat{\rho}_{\text{off}}$ in the system density matrix $\hat{\rho}$ by using an optical field. The system is subject to dephasing (loss of initial phase relationship in $\hat{\rho}_{\text{off}}$ without loss of amplitude) and decoherence (loss of amplitude in $\hat{\rho}_{\text{off}}$ caused by environmental factors not explicitly included in the system density matrix $\hat{\rho}$). For a sufficiently large system, one part of the system can serve as a bath for the other part, so dephasing of the two systems combined corresponds to a decoherence process of the reduced density matrix of each part. Both full density matrices undergoing dephasing ('pure states' and reduced density matrices undergoing decoherence ('impure states') will be discussed in different contexts.

The systems discussed here are described by a manifold of discrete quantum states. At first glance, dephasing in such a system seems like a trivial process: in the case of a pure nonstationary state $\rho(t) = |t\rangle\langle t|$, it results from the changing phases of its energy eigenstate components:

$$0 \leqslant P(t) = \mathrm{Tr}\{\rho(0)\rho(t)\} = \sum_i |c_i|^4 + 2\sum_{i<j} |c_i|^2|c_j|^2 \cos(\omega_{ij}t) \leqslant 1, \qquad (1)$$

where ω_I are the eigenvalues of the system and c_i are the amplitudes of the pure state $|t\rangle$ in the eigenbasis. The problem is that in coupled many-degree-of-freedom systems, the eigenvalues ω_I and corresponding eigenstates $|i\rangle$ bear no simple relationship to one another, and are difficult to compute. In the strong coupling limit, statistical analyses apply, and much has been learned about the behaviour of quantum states in that limit [4]. Yet statistical models such as the Gaussian orthogonal ensemble (GOE) model do not apply when there is only partial quantum chaos, i.e. when the coupling is not too strong [5]. This is the case for molecular

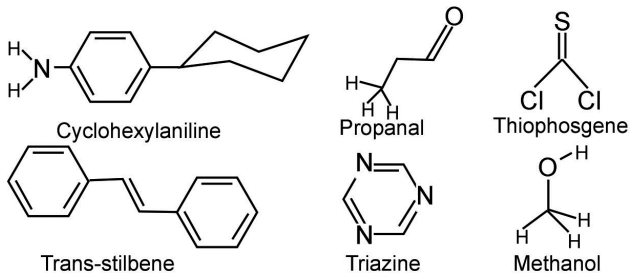

Figure 1. Six of the molecules discussed as examples in the text. Each node corresponds to a carbon atom, and each connecting vertex to an electron pair bond. Each carbon atom connects via four bonds, but not all bonds to hydrogen atoms (−H) are shown explicitly. Other atoms are shown explicitly (N = nitrogen, S = sulfur, Cl = chlorine, O = oxygen). Molecules such as cyclohexylaniline, propanal, stilbene, and methanol can undergo internal rotation motions with barriers ranging from 0.04 to 0.25 eV.

bonding. Dephasing therefore controls in nontrivial ways the time evolution of molecular vibrations [6]. Quantum control over dephasing by external fields can bring about desirable outcomes such as optical switching of vibrations [7], changing chemical reaction yields [8], and stabilizing desirable quantum states [9]. Instead of global random matrix models, explicit full-dimensional models or local random matrix models provide the necessary understanding of dephasing in these systems [10, 11]. As it turns out, if one looks at a single vibrational mode of even a small molecule, the other modes serve to decohere it, and a statistical limiting population of that mode is eventually reached. Thus molecules can act as their own heat baths, and serve as miniature condensed matter model systems with a controllable number of degrees of freedom, and optically controllable interactions [12].

When atoms interact to form molecules, only a small number of valence (weakly bound) electrons from each atom contribute to the binding energy. Although the electronic wavefunction is highly delocalized compared to the nuclear position wavefunction, chemical formulae generally depict nuclei as vertices connected by electron pair bonds localized between nuclei (figure 1). This 'Lewis' picture is correct only in the limit of 'heavy' electrons, but serves as a convenient shorthand for describing chemical bonding.

When the nuclear positions are distorted from the equilibrium geometry, the electronic energy increases. Near equilibrium, the electronic energy can be approximated by a quadratic function of the nuclear coordinates, which can be diagonalized to a normal mode representation. Thus, the atoms within the molecule vibrate collectively as a set of uncoupled harmonic oscillators. At higher energies, this approximation breaks down and anharmonic couplings appear between modes. There the energy is more conveniently expanded in local mode coordinates, with quadratic self-terms, cross-terms between adjacent bonds, between next-to-adjacent bonds, etc. In other words, forces can be described accurately as being transmitted through bonds or groups of nearby bonds. In this context it is important to note that atoms generally make only 1–4 bonds, with occasional exceptions up to eight-electron-pair bonds: the connectivity b of chemical formulae is relatively low, $b \approx 1$–8.

The vibrational Hamiltonian has a structure conducive to expansion in localized normal mode or local mode coordinates (section 2) [13, 14]. Higher order anharmonic couplings decrease rapidly with the order of the coupling and with the separation between the bonds displaced by the coupled modes. This scaling is exact in the limit of high nuclear masses and low molecular symmetry, in which case the normal modes are delocalized over just a few bonds [14, 15]. The majority of molecules fall into this category. As a result, correlations

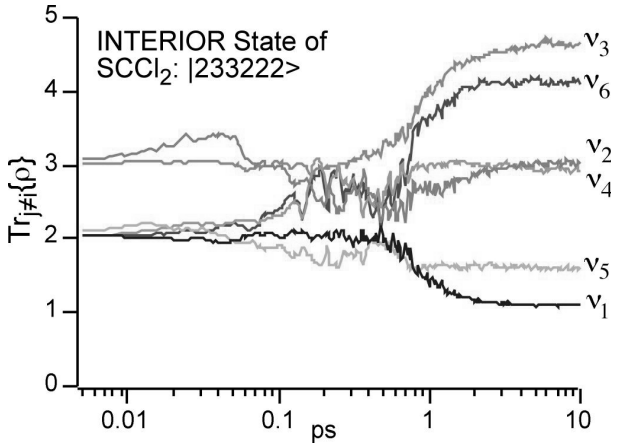

Figure 2. Single-point reduced density matrices for each of the six modes of $SCCl_2$ as a function of time, when a quantum state at ≈1 eV is excited. The populations decay to a Bose–Einstein distribution. Similarly, two-point reduced density matrices show a rapid decrease of the off-diagonal element, or decoherence of mode pairs by the remaining four modes as the Bose–Einstein distribution is reached (see figure 17 for a 2×2 example). Thus molecular modes form effective heat baths for one another at sufficiently long times. However, rather slow dynamics may be required to achieve this equilibrium situation, opening up the possibility of quantum control during the dephasing/decoherence process.

among couplings lead to an asymptotic slowdown of the dephasing dynamics [16, 17]. It is this slow dynamics that potentially allows dephasing to be controlled by external fields. This situation is significantly different from the delocalized or Fourier-space treatments used in the solid state, but is familiar from defect-rich systems (e.g. Anderson localization) [10].

Embedding a many-atom molecule in a condensed phase environment (e.g. a solution) adds an additional difficulty because of decoherence of any molecular wavepackets by the solvent environment. Nonetheless, coherent control has been observed in the condensed phase, such as in the localization of vibrational motions in methanol [7]. However, so far only very small deviations from a diagonal density matrix have been achieved in such cases. Simple models provide some insight into what timescale control of vibrational dephasing is irreversibly affected by solvent degrees of freedom [18].

Even in the absence of a solvent, large molecules act like miniature condensed matter systems: one set of modes can be considered as a bath for another set, leading to equilibration of mode populations according to Bose–Einstein statistics with an effective temperature $T \approx E/(kN)$, where E is the total excitation energy, k is Boltzmann's constant, and N is the number of degrees of freedom. Figure 2 shows such equilibration in thiophosgene, a molecule with only six vibrational degrees of freedom [12]: each of the modes is decohered by the remaining five if we look at single-mode reduced density matrices. In the 6D complete system density matrix, this process of course appears as dephasing only, as a reminder of the close relationship between dephasing and decoherence. This property suggests a model such as the 'Bose statistics triangle rule' (BSTR) model described later.

Molecular vibrations also provide a potentially attractive way of experimenting with few-qubit quantum gates. Nuclear magnetic resonance spectroscopy has been used to simulate quantum computing [19], but the spacing of energy levels is very small compared to kT, so density matrices remain nearly diagonal. Pure states and entanglement are more easily achieved with molecular vibrations in cooled molecules, where the energy scale can be large

compared to kT [20]. The timescale of vibrations (10 fs–1 ps) in isolated molecules is also long compared to those of primary relaxation mechanisms such as spontaneous emission.

2. The vibrational Hamiltonian

The coupling constants in the vibrational Hamiltonian obey scaling laws and can be approximately factorized. In this section the origin of these properties will be explored, their validity will be examined by comparison with accurate computational and experimental data, and a simple local random matrix model will be presented that mimics the properties of the vibrational Hamiltonian most important for understanding the dephasing dynamics.

2.1. Born–Oppenheimer approximation and the anharmonic oscillator model

The electronic–nuclear Hamiltonian for a molecule is given by [21]

$$H = K_{\mathrm{e}} + V_2(r_{\mathrm{e}}) + V_3(R_{\mathrm{n}}, r_{\mathrm{e}}) + K_{\mathrm{n}} + V_1(R_{\mathrm{n}}) \tag{2}$$

where K are the electronic and nuclear kinetic energies, and V_i the Coulomb operators for electron–electron repulsion, electron–nuclear attraction, and nuclear–nuclear repulsion. Equation (2) can be solved approximately by neglecting the slow nuclear degrees of freedom (adiabatic or Born–Oppenheimer approximation), yielding approximate nuclear equations of motion

$$H_i = K_{\mathrm{n}} + V_i(R_{\mathrm{n}}) \tag{3}$$

for each solution (electronic state) of the truncated equation (1). In the absence of external torque or centre-of-mass dependent forces, these equations can be represented for N atoms in an $\mathcal{N} = (3N - 6)$-dimensional manifold of nuclear degrees of freedom, and the potential energy becomes (the i will be dropped henceforth unless a specific electronic state needs to be referred to)

$$V = \sum_{n=2} \sum_{n_i} V^{(n)}_{[n_i]} \prod_{i=1}^{N} (a_i^{\dagger} + a_i)^{n_i} \tag{4}$$

where n is the overall order of a potential in the coordinates ($n = \sum n_i$) and n_i is the order of an individual unitless coordinate $q_i = a_i^{\dagger} + a_i$. The potential constants $V^{(n)}$ are sorted by order, and the subscript array $\mathbf{n} = [n_1, \ldots, n_N]$ indicates the order of individual unitless ladder operators. In a normal mode representation there are no quadratic cross-terms, whereas in a local mode representation there are such terms. In either representation, $V^{(2)} \sim \omega$, where ω is the vibrational frequency. This is the anharmonic oscillator model.

2.2. The scaling law and factorization of the coupling terms

The coupling constants of this model obey a simple scaling law. One can easily show using quantum mechanical or semiclassical arguments that electronic energies and vibrations are quantized with an energy ratio

$$\sqrt{\frac{V^{(n+1)}}{V^{(n)}}} \propto \sqrt{\frac{\hbar\omega}{D}} \propto \sqrt{\frac{m_{\mathrm{e}}}{m_{\mathrm{n}}}}, \tag{5}$$

where ω is a typical vibrational frequency (100 meV), D is a typical energy scale for dissociating a molecular bond (2 eV), and the masses are for electrons and nuclei. As a result, the potential constant $V^{(n)}$ of a given order n scales as [11, 14, 22]

$$V^{(n)} \propto \left(\frac{\hbar\omega}{D}\right)^{n/2} = c^n. \tag{6}$$

Thus two normal or local mode vibrational eigenfunctions $|\mathbf{n}\rangle$ and $|\mathbf{n}'\rangle$ of the quadratic approximation to equation (3) are strongly coupled only when their quantum number difference $n = \|\mathbf{n} - \mathbf{n}'\| = \sum |n_i - n_i'|$ is small.

Equation (5) also shows why we need to deal with the vibrational dynamics problem quantum mechanically instead of classically. A typical energy scale of interest for quantum control of chemical reactions, or for accessing sufficiently many states for quantum computing, is D. Although nuclei are reasonably massive, and vibrational energy level spacings ω are small compared to D, the ratio $D/\omega < 3N - 6$ for all but the smallest of molecules. Upon dephasing, the vibrational wavefunction acquires a character where mode populations obey Bose–Einstein statistics (see section 2.4 and figure 2); thus the average population per mode will be <1. This is clearly in the quantum limit. Although states with many nonzero mode quantum numbers can be coupled to many other states by ladder operators in equation (4), the couplings are relatively weak because the mode excitation is small.

The coupling constants can be written in a cumulant expansion that allows for approximate factorization. If we treat $V_{[n_i]}$ as a discrete function of the $3N - 6$ parameters n_i, the $\ln|V|$ expansion becomes [14]

$$\ln|V^{(n)}_{[n_i]}| = \sum_i n_i \ln|c^{(1)}_i| + \sum_{i,j} n_i\, n_i \ln|c^{(2)}_{ij}| + \cdots. \tag{7}$$

It has been shown using the central limit theorem and Wick's theorem that if $N \to \infty$ and if the local or normal mode vectors are Gaussian random variables (when expressed in space-fixed coordinates), then all terms but the first one in equation (7) vanish [14]. For real molecules, N is of course finite and the modes are not random, but (7) is so rapidly convergent that even the fully factorized version of equation (4),

$$V \approx \sum_{n=2} \sum_{[n_i]} (\pm 1) \prod_{i=1}^{N} c_i^{n_i} (a_i^{\dagger} + a_i)^{n_i}, \qquad c_i \sim D_i^{1/n} \sqrt{\omega_i / D_i}, \tag{8}$$

produces good results for highly connected molecules (section 2.4). It has also been shown by using semiclassical connection formulae that such scaling and factorization apply to modes which are better represented by a rotor than by an oscillator Hamiltonian [23]. An example would be the torsion of the H_2N group around the N–C bond or the torsion of the HO group around the O–C bond in the first and last molecules of figure 1. The arguments presented here thus cover all types of internal molecular motion. The important messages of this section are therefore: couplings decrease exponentially quickly with coupling order, can be factorized approximately, and the dynamics must be dealt with quantum mechanically at the energies of interest.

2.3. Symmetry breaking and factorization of the couplings

There is one important exception where at least the second term in equation (7) must be considered to obtain accurate coupling constants: when symmetry is broken, mixed coupling constants become much smaller than self-coupling constants [15]. Consider the chain molecule in figure 3, with two local C–H stretching modes at opposite ends. The first term in equation (7) implies that $\bar{V}^{(3)}_{[1,2]} = (V^{(3)}_{[3,0]} V^{(3)^2}_{[0,3]})^{1/3}$. In that case the local modes would be strongly coupled, resulting in symmetric phase and antisymmetric phase delocalized modes. This is true if the molecule is perfectly symmetrical. It has been shown that upon even a small symmetry breaking (e.g. by substituting a deuterium for a hydrogen somewhere along the chain) the modes become localized. The sensitivity of delocalized modes to symmetry breaking grows

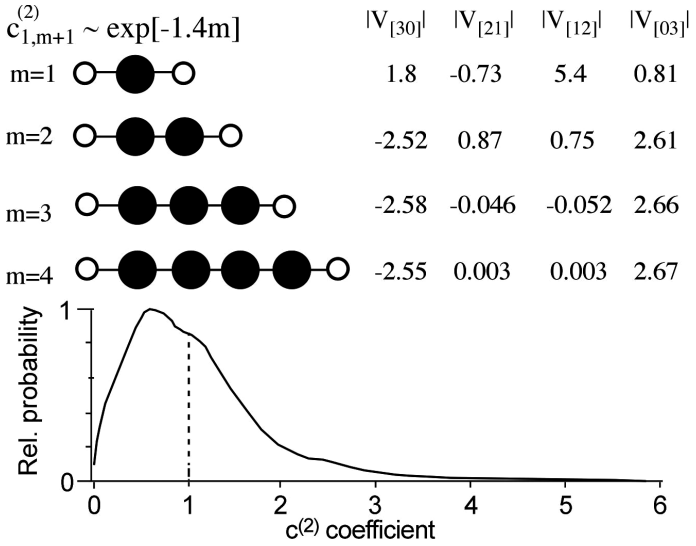

Figure 3. Slight symmetry breaking introduces strong localization of modes. In the hypothetical chain molecule shown, the force constants k of the two terminal stretching modes differ by 5%, typical of organic molecule C–H stretching modes. In a short chain the mixed coupling constants are comparable to the local coupling constants. By $m = 4$ the mixed couplings are negligible compared to the local coupling constants, and the two modes have completely localized. Bottom: distribution of localization coefficients $c^{(2)}$ for a large number of organic molecules [15].

exponentially with the number m of bonds intervening between the principal groups of atoms involved in the motion, so

$$V^{(3)}_{[2,1]} \approx V^{(3)}_{[1,2]} \sim \bar{V}^{(3)}_{[3,0]} {c^{(2)}_{1,2}}^2 \sim \bar{V}^{(3)}_{[3,0]} f^{-m} < \bar{V}^{(3)}_{[3,0]} \approx \bar{V}^{(3)}_{[0,3]} \tag{9}$$

where $f \approx 2$–3. The same effect has also been found for internal rotor modes: vibrational modes that in the harmonic approximation move atoms close to a rotor mode are more strongly coupled to it. It is also possible for symmetry lowering to mediate accidental resonances, so $c^{(2)} > 1$. The ratio of actual coupling constants to the factorized couplings predicted from equation (6) can be used to estimate the distribution function of $c^{(2)}$ with the assumption that higher order corrections are significantly smaller. The distribution is shown in figure 3 for a large number of organic molecules [15].

2.4. Comparison with computed and experimental coupling constants

Based on the observations made in sections 2.2 and 2.3, a class of scaled and factorized force fields has been developed for computing dephasing properties of optically excited molecules. These force fields use only minimal information about the molecule, such as the local or normal oscillator frequencies, dissociation energies D of various bonds, spatial overlaps between modes, and anharmonicity parameters c_i. The models in the preceding sections have been compared with molecular data. For example, the scaling of coupling constants from an experimentally fitted vibrational potential surface of thiophosgene is compared to equation (6) in figure 4 [24]. *Ab initio* quantum calculations for the anharmonic couplings of a rotor mode in aldehydes of different chain length (figure 1) to other vibrational modes are compared to the overlap of atomic displacements in figure 4 also [23]. Modes with smaller spatial overlap in the harmonic approximation have smaller couplings, as predicted.

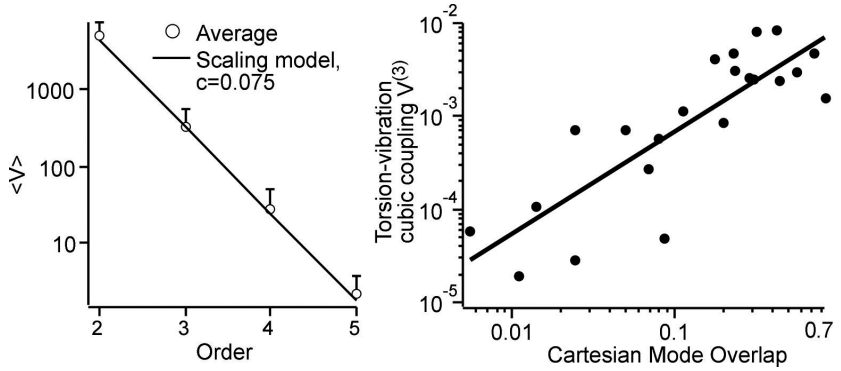

Figure 4. Left: coupling constants of $SCCl_2$ up to fifth order, evaluated from a vibrational Hamiltonian fitted to over 100 vibrational energy levels. An exponential fit with scaling constant $c = 0.075$ is also shown. Right: correlation between the cubic coupling strength between the terminal internal rotation of propanal and similar aldehydes (figure 1) and other vibrational modes, correlated with the spatial overlap of the internal rotation and vibrations.

2.5. A minimal random matrix model: the BSTR model

We can arrive at a minimal local random matrix model for vibrational dephasing by taking into account equation (7) and remembering that vibrational quanta are bosons (figure 2) [6, 25]. A molecule with vibrational modes populated by vibrational quanta is analogous to a cavity populated by photons. Vibrational quantum number populations of modes relax towards the Bose–Einstein distribution because of the couplings in equation (7), and photon populations relax towards the Bose–Einstein distribution because of creation/annihilation at the thermal cavity wall; the difference is in the distribution of mode frequencies. The 'Bose statistics triangle rule' model posits the following simple rules for the Hamiltonian matrix [25]:

(1) The H_{ii} are Poisson distributed with average spacing $\rho(E)^{-1}$.
(2) $H_{ij} = \pm V c^{n_{ij}}$, where n_{ij} is the quantum number difference between states $|i\rangle$ and $|j\rangle$.
(3) n_{ij} is normally distributed with mean $\bar{n} = E/\bar{\omega}$ and variance $\sigma_n^2 = 2E^2/(3N-6)\omega^2$.
(4) For any triplet i, j, k, $|n_{ij} - n_{jk}| \leqslant n_{ik} \leqslant |n_{ij} + n_{jk}|$.

Rule (1) is satisfied for uncoupled harmonic oscillators with irrational frequency ratios. Rule (2) follows from equation (6). Rule (3) is required to achieve a Bose–Einstein distribution at long times. The triangle rule (4) requires more explanation: if two states have a small quantum number difference and a third state has a large quantum number difference from one of them, it will also have a large quantum number difference from the other one (figure 5). This rule has to be rigorously satisfied by the vibrational quantum numbers; because H_{ij} is monotonic in n_{ij}, a similar rule is satisfied by ratios of coupling matrix elements, but only to the extent that (2) holds. Comparison with electronic structure calculations and experimentally measured couplings shows that the rule is satisfied by 80–90% of coupling matrix elements in practice [6, 24].

The BSTR model qualitatively reproduces all the results obtained with experimentally derived or accurate computational Hamiltonian operators (section 4). It can only be used to follow statistical trends for an ensemble of molecules because it only contains highly averaged molecular quantities such as V, c, and $\bar{\omega}$. Its dephasing function $P(t)$ and other properties differ very much from the behaviour of a Gaussian orthogonal ensemble (GOE) matrix because rules (2) and (4) force states to be coupled hierarchically. Of course, a GOE matrix can always

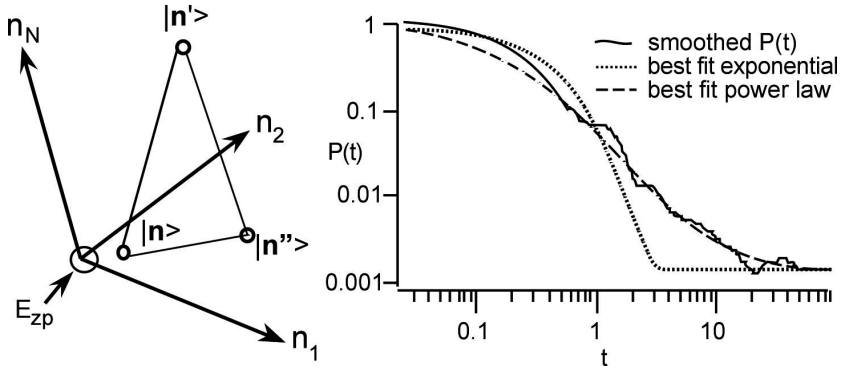

Figure 5. The origin of the triangle rule in state space. If coupling elements scale as $Vc^{n_{ij}}$, where n_{ij} is the quantum number difference between a pair of states, then the couplings will also obey a triangle rule. The BSTR simulation for a 9D system of oscillators obeying the rules in section 2.5 shows a sub-exponential decay of the dephasing function $P(t)$.

be brought into the form of a BSTR matrix by a unitary transformation, but its eigenvectors will be random linear combinations of the BSTR eigenvectors that cannot be achieved as initial states of the dynamics for reasons discussed in the next section.

3. The vibrational state space

In this section we discuss the concept of the vibrational state space [11, 16], which is useful because of the structure of the Hamiltonian inherent in equation (7) or in the BSTR rules. The advantage of the state space is that it allows easy visualization of the consequences of equation (7), much in the same way that Feynman diagrams are generally easier to follow than the corresponding written-out path integrals.

3.1. State space structure and the state density

In classical mechanics, action variables are useful for representing the phase space, particularly if some of the actions are conserved or only slowly varying as a function of time (near-invariants of the motion). Quantum mechanically, this translates into a state space with quantum numbers $n_i \sim J_i/\hbar$ [4]. For a molecule with $3N - 6$ vibrational degrees of freedom, the state space is $3N - 6$ dimensional. Because the couplings decrease rapidly with order, it makes sense to label the state space with normal mode or local mode quantum numbers. Of course, not all of these will be preserved as good quantum numbers. Each state or 'cell' in state space occupies a volume of roughly $\hbar^n$.

Figure 6 shows a depiction of three of the N dimensions of a molecular state space. Each local or normal mode state is labelled by a vector $\mathbf{n} = [n_1, n_2, \ldots, n_{3N-6}]$, and the 1-norm n_{ij} of the difference between two vectors is the quantum number difference between two states. The states are not eigenstates, but as discussed in section 3.2, ultrafast optical excitation can access a subset of these states. In principle, the vibrational wavepacket then is free to expand in N dimensions under the unitary time evolution operator. If the excitation pulse is sufficiently narrow band, then only the energy shell is accessible to dephasing by energy conservation, and energy flow is restricted to $N - 1$ dimensions. The energy shell appears as a triangular facet in the positive octant in figure 6.

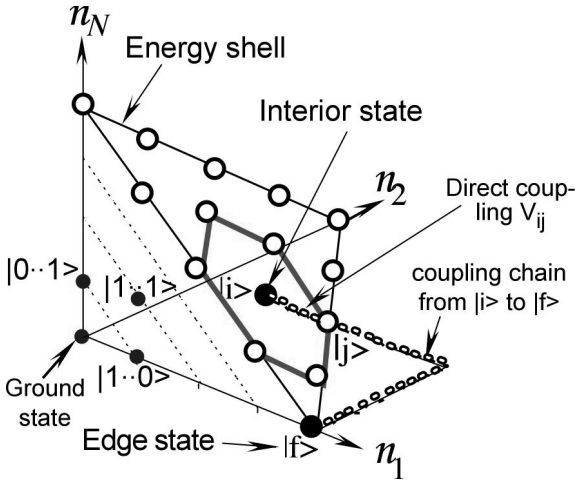

Figure 6. State space showing three of the quantum number (action coordinate) axes. The red (grey in print) hexagon shows states that contribute to the local density of states of state $|i\rangle$. States $|i\rangle$ and $|j\rangle$ are coupled directly, $|i\rangle$ and $|f\rangle$ via a coupling chain. In real molecules irrational relationships between the frequencies cause the states or 'cells' in state space to not exactly lie on the energy shell, as shown here. Also shown in blue (black ● in print) are four states that can represent a coupled two-qubit system as described in the text.

Three important concepts for understanding the dynamics are the total density of states on the energy shell, the local density of states on the energy shell, and the local number of coupled states. The total density of states in state space is simply given by

$$\rho(E) = \frac{1}{\Delta E} \sum_{\mathbf{n}} \delta_{\mathbf{n}}(E, \Delta E), \tag{10}$$

where the function $\delta_{\mathbf{n}}(E, \Delta E)$ equals 1 if the state space point $\mathbf{n}$ is located in the half-open interval $[E - \Delta E/2, E + \Delta E/2)$, and 0 otherwise. By choosing the interval ΔE sufficiently large, ρ can be represented as a relatively smooth function. It has been shown that this function can be expanded in a series of moments of the vibrational frequencies ω_I, and the leading term is [15]

$$\rho(E) = \frac{\sqrt{3N-6}\Gamma(E/\hbar\bar{\omega} + N)}{\Gamma(E/\hbar\bar{\omega})\Gamma(N)\hbar\bar{\omega}}, \tag{11}$$

with $\bar{\omega}$ being the average molecular vibrational frequency in units of rad s^{-1}. Unlike semi-empirically modified semiclassical expressions, this expression scales correctly for all limits of E and N.

The local density of states $\rho_{\mathbf{n}}^{(n)}(E)$ on the energy shell is the number of states surrounding a state with vector $\mathbf{n}$ at a distance n. In figure 6, it is shown by a hexagon about state $|i\rangle$. The reason that this function is generally more relevant than the total density of states is that states are coupled only locally according to equation (7), so quantum amplitude can flow only locally. The expansion for the local density of states analogous to equation (10) is [15]

$$\rho_{\mathbf{n}}^{(n)}(E) = \frac{\sqrt{N}\pi_{N-1}\pi_N}{(N-1)!\bar{\omega}} n^{N-2} f_{\mathbf{n}}(E) + \mathrm{O}(n^{N-3}) \approx \frac{N^{n+1/2}}{(n/2)!^2\bar{\omega}} f_{\mathbf{n}}(E). \tag{12}$$

Here $0 < f_{\mathbf{n}}(E) \leqslant 1$ is a function which is less than unity if $\mathbf{n}$ is a vector within distance n of the edge of state space because no states exist outside the positive octant in figure 6, and

π_N is the Nth prime. The approximation holds in the common case where $n < N$. Unlike $\rho(E)$, $\rho_{\mathbf{n}}^{(n)}(E)$ scales only as a low order polynomial of the dimension N of the state space; it does not increase significantly with energy.

The third concept, closely related to the local density of states, is the local number of coupled states. This number is a measure of how many nearby states a state $|i\rangle$ directly mixes with. In addition to the coupling strength, it takes into account that states need to be nearby in energy in order to mix: they need to be in resonance. For example, assume that the Hamiltonian contains a term $V_{[1,2]}^{(3)} a_1^\dagger a_2^2$. This term mixes states $|n, m\rangle$ and $|n+1, m-2\rangle$, but the mixing will be weak unless the states are in resonance. In the harmonic approximation, this means that $\omega_1 \approx 2\omega_2$ so $E_1 \approx E_2$. The perturbative criterion [11]

$$L_{ij}^{(n)} = \{1 + (\Delta E_{ij}/V_{if}^{(n)})^2\}^{-1/2}, \tag{13}$$

which varies between 0 and 1, can be used to assess whether a state $|j\rangle$ is strongly coupled to a state $|i\rangle$. In equation (13), ΔE_{ij} is the energy gap between states $|i\rangle$ and $|j\rangle$, and $V^{(n)}$ is the nth-order coupling connecting the states. It has been shown that the local number of coupled states scales as [15]

$$N_{\mathbf{n}}^{(n)}(E) \approx 2 \ln 2 \rho_{\mathbf{n}}^{(n)} V c^{n-3} \overline{c^{(2)}} (E/\bar{\omega})^{n/2}. \tag{14}$$

This function increases with energy, albeit polynomially, and therefore much more slowly than $\rho(E)$. A related criterion T has been derived by analytical mean field theory [10, 26]. The locally coupled states do not uniformly fill out state space around the state $|\mathbf{n}\rangle$ [11, 27]. Modes are localized and couplings are transmitted through small groups of bonds, so only a small number $\Delta \ll N$ of resonances is active at any given position in state space (the maximum number of linearly independent resonances is of course N). If modes were localized to single bonds and f in equation (9) is large, then the number of resonances would not exceed the connectivity of the molecular formulae, about 1–4. In reality not all bond vibrations are in resonance (this tends to decrease the number further), but modes are more delocalized and $f \approx 2$–3 (this tends to increase the number of resonances). The combination of branching $b \approx 1$–4 and an exponential fall-off of couplings e^{-m} with the number of bonds (equation (9)) results in $\Delta \approx 2$–4 resonances being active at any point in state space, even in large molecules (as long as their symmetry is sufficiently low). This is very different from the usual condensed phase 'lattice' limit, where very long range collective modes can exist, undisturbed by defects. From this perspective, the vibrational heat capacity of large molecules should behave more closely according to Einstein's formula than Debye's formula, just like glasses do.

3.2. Edge states, interior states, and feature states

The function $f_{\mathbf{n}}(E)$ is dependent on the position of a state within state space. This positioning has important effects on the local dynamics [28], and we distinguish two general classes of states: edge states such as $|f\rangle$ in figure 6 have excitation in only one or a few modes, while interior states such as $|i\rangle$ have excitation in many or all modes [11]. Neither edge states nor interior states are eigenstates of the vibrational Hamiltonian (4). Under unitary time evolution, amplitude will leak into nearby states, so the dephasing function or 'survival probability' $P(t) = |\langle 0|t\rangle|^2$ of equation (1) will decrease. At a given energy E, the dephasing of edge and interior states is restricted for different reasons. Edge states are restricted by the state space boundaries: only a small number of nearby states is available because $f_{\mathbf{n}}(E) \approx 0$. Interior states are restricted by weaker couplings: the many modes are each populated by a small number of quanta $n_i \approx E/[N\omega_i]$ even as E approaches the molecular bond dissociation energy D, so modes are more nearly harmonic. According to equation (14), edge states are more strongly coupled to a smaller number of states, and interior states are more weakly

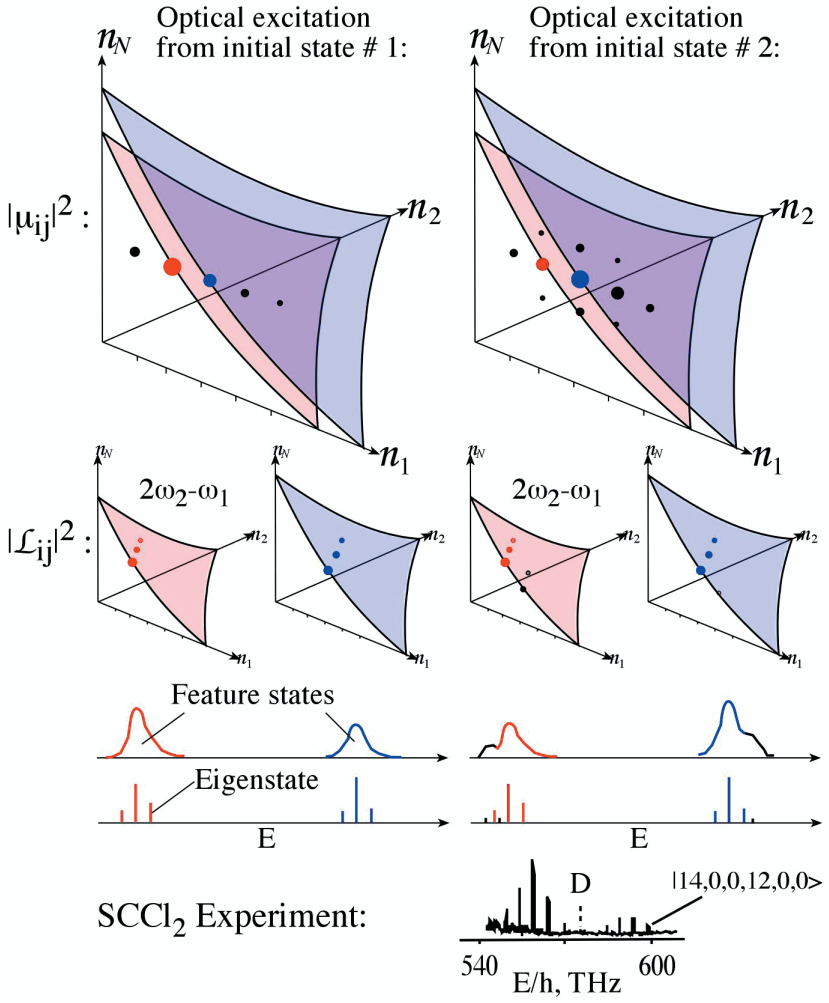

Figure 7. Both dipole and vibrational coupling operators are local in state space. Top row: feature states accessed by the dipole operator; the left shows a transition active in only one mode (5 features), the right, one active in two modes according to equation (15) (11 features). Two energy shells are shown in blue and red; only states on the same energy shell are excited simultaneously by a narrow band optical pulse (1 feature on each left energy shell, 2 features on each right energy shell). Next row: the coupling operator mixes optically accessed features with other states along the direction $2\omega_2 - \omega_1$. Couplings are shown on the lower (red) and higher (blue) energy shells. Next row: low resolution spectra of the feature states and high resolution spectra of the underlying eigenstates that light up in the spectrum. On the left-hand side, only one feature lights up on each energy shell; on the right-hand side, two features overlap on each energy shell (red/black and blue/black). Bottom row: experimental data for the molecule $SCCl_2$, showing 9 features, one labelled, with 6 quantum numbers, by its location in state space ([24]).

coupled to a larger number of states. The existence of edge and interior states distinguishes local random matrix models such as the BSTR model from global random matrix models such as the GOE one, where all states have a statistically equal likelihood of being connected.

The most important state space concept from the point of view of optical excitation is the feature state (figure 7), a group of eigenstates which shares the same source of oscillator

strength to 'light up' upon optical excitation [12, 29]. If the local or normal mode states in vibrational state space were very strongly mixed, and if optical transitions accessed states uniformly in state space, spectra obeying GOE statistics would be observed. Instead, one finds highly regular features in spectra even at the energy scale D, as illustrated at the bottom of figure 7 with experimental data from $SCCl_2$ (figure 1) [24]. These features are arranged in hierarchical patterns (groups of states within groups) discussed in section 4. This regularity results from a cooperation between the local couplings and the locality of the dipole operator in state space.

Optical transitions between molecular states occur via a transition dipole operator $\hat{\mu}$. Like the potential energy surfaces $V_i(R_n)$ in equation (3), the dipole operator is a slowly varying function of the nuclear coordinates. Therefore the transition dipole matrix elements also fall off rapidly when two states $|i\rangle$ and $|j\rangle$ have a large separation in state space:

$$|\mu_{n,n'}|^2 = |\langle \mathbf{n}|\hat{\mu}|\mathbf{n}'\rangle|^2 \propto \prod_{i=1}^{N} c_{\mu i}^{|n_i - n_i' - n_{0i}|}. \tag{15}$$

This equation is analogous to equation (7), except for the introduction of an offset $\mathbf{n}_0$. The offset is 0 if the initial state $|i\rangle$ is the ground state and the optical pulse is in the infrared. Infrared pulses ($E \approx \hbar\omega$) can excite only a few vibrational states near the ground state. The offset is nonzero if visible or UV pulses ($E \approx D$) are used to make a transition from one electronic surface $V_i(R_n)$ to another electronic surface $V_j(R_n)$ of equation (3). The reason is that different electronic surfaces V_i have different structures (equilibrium positions of the atoms) and vibrational frequencies, so vibrational states offset by $\mathbf{n}_0$ have maximum overlap (the Franck–Condon principle; strictly speaking two electronic surfaces may have several vectors $\mathbf{n}_0$). Because electronically excited states differ only locally in structure (the low molecular symmetry at work again), the vector $\mathbf{n}_0$ is close to zero for most degrees of freedom. This is illustrated in figure 7. Thus even transitions between different electronic surfaces access regions of state space near the edges because the initial state must be thermally populated and hence near the origin of state space.

More of the state space can be accessed by 'multi-resonance' experiments [30, 31]. For example, a sequence of two optical pulses from electronic state V_i up to V_j and back down to V_i can access states with large quantum numbers in some modes. This is known as a 'double-resonance' experiment. Every additional light pulse digs a little deeper into state space [31]. Experiments up to triple resonance have been performed, but truly interior states of large molecules have not been accessed optically, and assigned feature states are generally edge, near-edge states, or combinations of a few edge states that share oscillator strength.

Equation (15) ensures that spectral intensity is carried by well-defined regions of state space, and equations (6) and (13) ensure that dephasing does not cause the spectral intensity to leak far out of these regions. As a result, feature states such as the ones shown in figure 7 can contain many eigenstates, but these share the same source of oscillator strength from a localized set of states in state space. In section 4 it will be seen that optically accessible feature states decay even more slowly than interior states, although the dynamics for the latter is also restricted because they contain few quanta per mode. In the spectrum this means that even when all eigenstates are observed in an energy window (access to the full density of states exists), many will contribute to the feature rather weakly.

3.3. Resonances and dynamical tunnelling (superexchange)

From the above discussion, one mechanism for dephasing an initially prepared feature state is obvious: the local couplings transport amplitude around the state space, fanning out from an

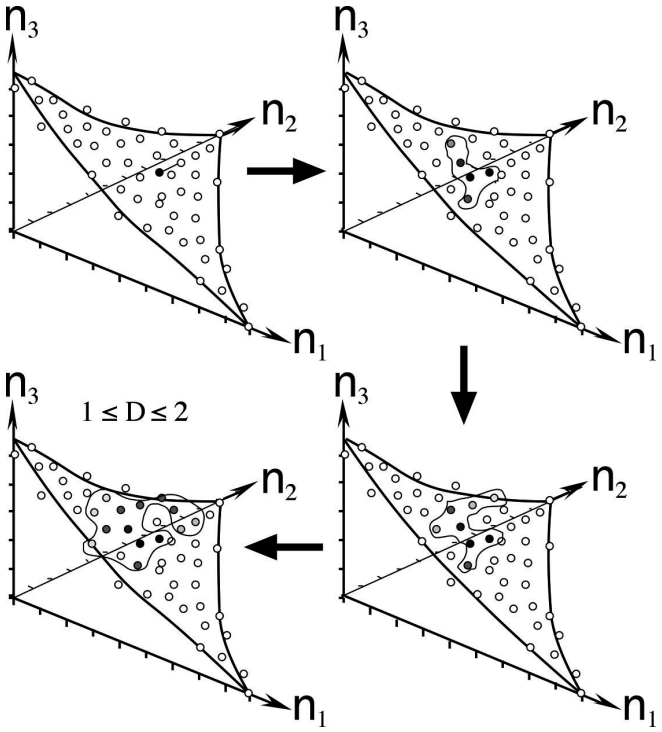

Figure 8. Resonant quantum diffusion in state space (anticlockwise). In the three-dimensional state space shown here, the vibrational wavepacket diffuses on a manifold of fractional dimension between 1 and 2. One-dimensional reduction is caused by energy conservation (two-dimensional energy shell). Further reduction is caused by localized couplings, so not all directions on the energy shell can be accessed from every point (see figure 7 also). Nonresonant diffusion via superexchange is also possible if the system is very near the threshold for energy flow.

initially excited feature state. This resonant mechanism of quantum diffusion [16], shown in figure 8, is operative when the energy is high enough that the local number of coupled states in equation (14) exceeds 1. Equation (14) has the form of a local density of states times a coupling strength, so free dephasing occurs when this product becomes large enough.

One question arises in connection with this dephasing mechanism: are high order couplings directly connecting two states or chains of lower order couplings indirectly connecting them more important contributions to the dephasing process? Two effects compete: low order couplings are larger and there are many chains connecting a pair of states; this favours chains. Chains can suffer phase cancellation if different paths between two states have opposite phases [15]. This is best illustrated by a 4×4 matrix toy model. Consider the matrix

$$H = \begin{pmatrix} 0 & 1 & 1 & 0 \\ 1 & 5 & 0 & 1 \\ 1 & 0 & 5 & -1 \\ 0 & 1 & -1 & 10 \end{pmatrix}. \tag{16}$$

States 1 and 4 are coupled via two equally strong coupling chains $1 \to 2 \to 4$ and $1 \to 3 \to 4$. Each chain by itself mixes states 1 and 4 significantly in the eigenstates near $E = 0$ and 10, but together they cause no mixing at all because of the -1 phase factor in the $1 \to 3 \to 4$ chain. Although this is an extreme example, this effect causes the importance of coupling chains to grow as the root of the number of chains only. Coupling chains and direct couplings generally

make comparable contributions, especially to the long time dynamics. As a general rule, direct higher order couplings are more important if the local density of states is increased by raising E, not N.

Dephasing thresholds as a function of energy are often lower than expected from direct couplings or direct coupling chains [32]. In other words, feature states consisting of several eigenstates can be observed even when resonant couplings are too weak to allow dephasing of a feature state. In that case, a different mechanism is operative: superexchange (also called dynamical tunnelling or doubly off-resonant coupling) [33, 34]. In superexchange, two states on the energy shell are connected by states far off the energy shell, and mix with each other, but not with the off-resonant state. Again, this mechanism is most easily illustrated by a toy model. Consider the matrix

$$H = \begin{pmatrix} 0 & 0 & 10 \\ 0 & 0.1 & 11 \\ 10 & 11 & 1000 \end{pmatrix}. \tag{17}$$

States 1 and 2 are not coupled directly, only off-resonantly though state 3. The eigenvectors for the system are approximately $(0.82, 0.58, -0.01)$, $(0.51, -0.87, 0)$, and $(-0.01, -0.01, 0.999)$, indicating that the two nearly degenerate states are strongly mixed by superexchange [35]. This mechanism still maintains locality of the feature state in state space: the strongest couplings still correspond to two small changes in quantum number from $1 \rightarrow 3 \rightarrow 2$, even though a coupling chain dominates over a small higher order coupling in this case. Figure 9 shows an experimental and computational example of this for the molecule triazine [35]. The superexchange mechanism is more likely for edge states than for interior states. Thus it does not dominate the dynamics at long times, or once the energy has increased sufficiently for direct couplings to contribute [15]. Skeletal vibrations (involving the heavy atoms, such as carbon, nitrogen, oxygen, and higher mass atoms) leave the superexchange limit faster than hydrogenic stretching modes.

4. Dephasing dynamics

Sections 2 and 3 provide the framework for understanding the dephasing dynamics of vibrational states, or decoherence of mode dynamics (for few-mode density matrices such as in figure 2). In this section we examine some formal analytical results, computational data, and experimental measurements of the dynamics. The dephasing dynamics is not described by global statistical models even when $E \approx D$. Although the survival probability in equation (1) generally approaches the statistical limit above the threshold energy for dephasing, it does so much more slowly than predicted by global statistical models.

4.1. Short time, asymptotic behaviour, and perturbation theory

The behaviour of equation (1) is trivial in certain limits [36]. Assuming the state is normalized such that $\sum |c_i|^2 = 1$, then as $t \rightarrow 0$ the time evolution becomes

$$P(t \rightarrow 0) = \cos\left[\sqrt{\sum |c_i|^2 |c_j|^2 \omega_{ij}^2}\, t\right]. \tag{18}$$

A finite-size quantum system not in the continuum has a roll-off phase in accord with short time perturbation theory. At long times, the limit of equation (1) averaged over a short time window simply becomes

$$\bar{P}(t \rightarrow \infty) = \sum |c_i|^4 = \sigma = N_{\mathrm{p}}^{-1} \leqslant 1. \tag{19}$$

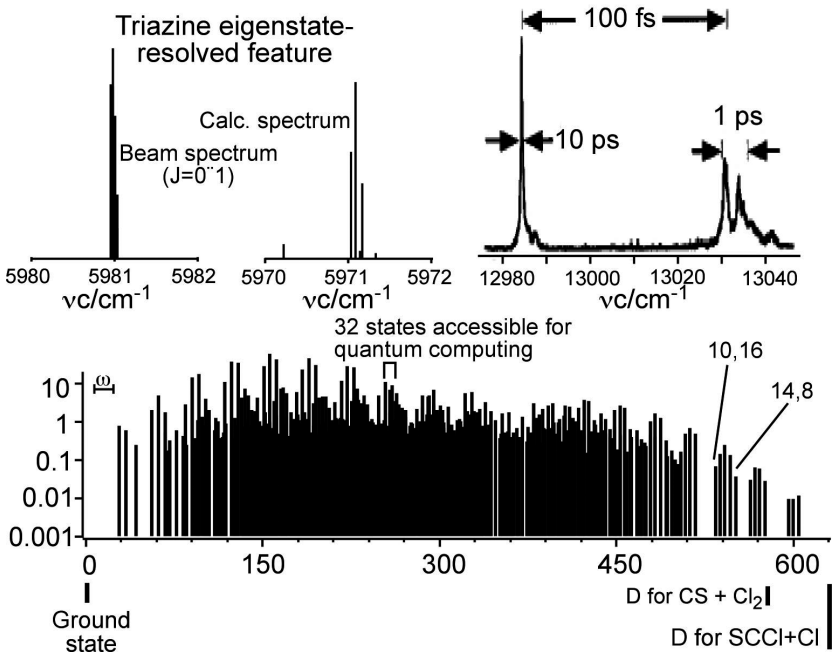

Figure 9. Spectral structure caused by vibrational dephasing. Top left: two quanta of excitation in a CH stretch of triazine (figure 1), showing how the feature is already distributed over several eigenstates, just above the threshold for dephasing ($N^{(3)} \approx 1$ in equation (14)). The calculation is a 21-dimensional filtered basis window diagonalization using the Mandelstahm–Taylor algorithm based on work by Neuhauser. Top right: the hierarchy of timescales in the experimental vibrational spectrum of methanol (figure 1) obtained by Rizzo and co-workers. Bottom: experimentally measured vibrational states of $SCCl_2$ up to dissociation. Energy scales for ω and D are indicated, as well as nominal mode populations in the stretching and out-of-plane bending vibration for two highly excited states. The bracket above the spectrum indicates the window size accessible by commercially available pulse-shaped titanium:sapphire femtosecond lasers for phase manipulation during quantum control. The window contains >32 states and can simulate a five-qubit system.

Although the summation in the second term of equation (1) contains more terms, the $\cos[\omega_{ij}t]$ behave like a collection of random variables, so the fluctuations as $t \to \infty$ are in fact of order σ. σ is known as the dilution factor and describes over how many eigenstates N_p a feature in the spectrum has been diluted.

At intermediate times, the dynamics deviate nontrivially from perturbation theory. The prediction of first-order perturbation theory, assuming that the coupling matrix elements are random Gaussian variables, is that

$$P(t) = (1-\sigma)\mathrm{e}^{-kt} + \sigma, \qquad k = \frac{2\pi}{\hbar}\rho(E)\langle V\rangle^2, \tag{20}$$

where $\langle V\rangle^2$ is the coupling variance.

4.2. Anisotropic quantum diffusion

The assumption of random Gaussian variables is not justified when couplings scale according to equation (7) or the rules in section 2.5 are obeyed [25]. Couplings fluctuate more strongly with energy and are more likely to be small near edge states. Thus equation (20) can be valid

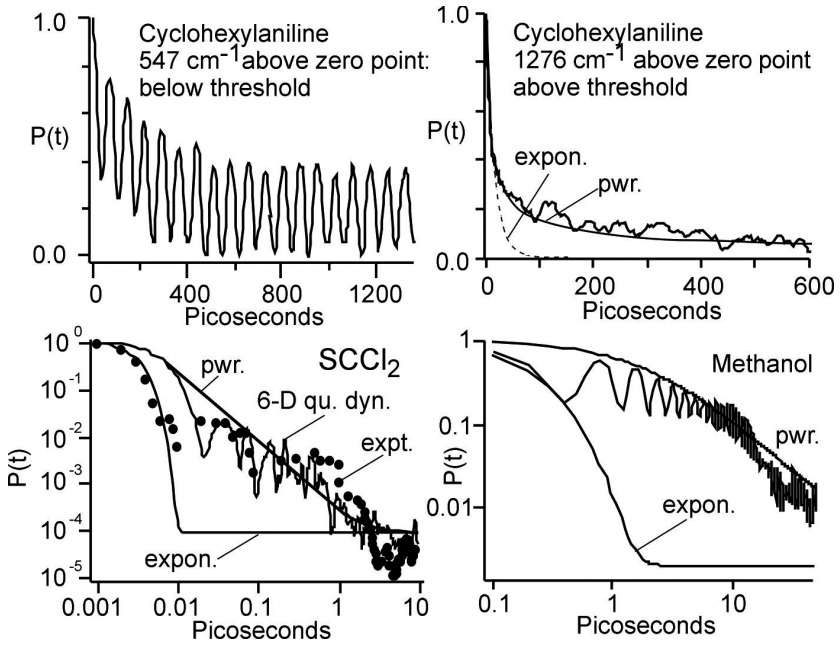

Figure 10. Comparison of experimental dephasing with the golden rule, power law models, and quantum dynamics calculations. Top right: cyclohexylaniline above the dephasing threshold; data from [39], analysis from [17]. Bottom left: the most extensive experimental data and quantum dynamics simulations are available for $SCCl_2$ [12]. Bottom left: methanol decay corresponding to figure 9, as calculated in [76].

only at short times. Scaling arguments and a one-step renormalization treatment show that the dephasing function is instead given by [12, 37];

$$P(t) = (1-\sigma)\left(1+\frac{t}{\delta/2}\right)^{-\delta/2}, \qquad \delta = \frac{\partial \ln \bar{N}^{(n)}}{\partial \ln n}, \tag{21}$$

where n is the distance in state space, and $N^{(n)}$ is defined in equation (14). δ is thus the fractal dimension of the manifold of locally coupled states. In a molecule with N modes where states are coupled in all N directions in state space subject to energy conservation, $\delta = N - 1$. Equation (20) would then be recovered for large N. As discussed in section 3.1, only a small number Δ of resonances are usually significant at any given point in state space, so we expect $\delta \approx \Delta \ll N$ to hold. The approximate equality should hold because states are coupled by resonances, and locally coupled states therefore occur in state space only in the direction of resonances [12].

The factor $1/2$ in equation (21) results from the assumption of random phase cancellation among coupling paths because of the signs in equation (8). As seen in figure 4, this assumption is justified when couplings are computed using accurate *ab initio* models for the molecular electronic structure. Figure 10 shows experimentally measured dephasing dynamics for three of the molecules in figure 1, excited with an average energy of 0.8–2 eV $\approx D$ [12, 17, 38, 39]. The result shows the initial decay, an exponential deflationary phase where the short time perturbation theory matches experiment, and subsequent power law dynamics until the baseline σ is reached. Oscillations or 'quantum beats' are superimposed on the decay; in fact, the first oscillatory decay which matches the exponential phase can be thought of as a quantum beat

that occurs before states near the feature are sufficiently populated for return flux of amplitude, and hence destructive interference, to occur. Quantum beats are always present because of destructive interference illustrated by the toy model matrix in equation (16). Their magnitude is proportional to σ as $t \to \infty$, and $D(t)^{-1}$ at other times (D is defined in section 4.5).

Figure 5 shows dynamics computed from the local random matrix BSTR model of section 2.5 [25]. The model also has a power law tail. It has been shown that a GOE-like exponential decay or decay with a coherence hole is obtained if rules (2) or (4) in section 2.5 are relaxed. Another way of interpreting the BSTR dynamics is that only a small fraction of the N quantum numbers required to describe the oscillator system break down severely. The remaining quantum numbers are approximately conserved locally. Which ones are conserved can be different in different parts of state space.

4.3. Energy thresholds

An important prediction of equation (21) is an energy threshold for dephasing [10, 11, 16, 32]. The local number of coupled states depends on energy. At low energy, where the local density of states is small and couplings are also smaller (the system is more harmonic), $\bar{N}^{(n)} < 1$ for all values of n. As a result the fractal dimension of the coupling manifold drops below 1, and the vibrational states become Anderson localized [10]. Each optically addressable feature contains only one eigenstate, and no dephasing can occur. Figure 9 shows the spectrum of a molecule just above that threshold: if the couplings of triazine are reduced by 30% from the value used to compute figure 9, no dephasing occurs [35]. The other example in figure 10 illustrates this in the time domain: below the threshold for dephasing, $P(t)$ for cyclohexylaniline (figure 1) is highly oscillatory because the feature contains only two eigenstates; above the threshold, a much smoother decay is observed because the feature now covers many eigenstates [39]. However, despite the fact that the latter feature state contains all the eigenstates in that energy region, and therefore accesses a statistical mixture of eigenstates at long time, the dephasing is still slow.

4.4. Feature state dilution

As discussed earlier, feature states are groups of eigenstates that share the same transition strength because the dipole and coupling operators are both local in state space. An important statistical measure of dephasing via local couplings is the dilution factor σ, already defined in equation (19) as the long time average of $P(t)$. According to equation (19) it equals the sum of the squares of the normalized spectral intensities $I_i = c_i^* c_i$. The GOE model predicts that as energy increases, the probability distribution for σ gradually shifts from peaked at 1 to peaked at 0 as features 'dilute' over many eigenstates. The BSTR model as well as analytical mean field calculations predict that the probability distribution is bimodal, that is, a state undergoes either no dephasing or strong dephasing, but intermediate cases are rare [40–42]. The latter is borne out by a comparison with experimental data (figure 11).

Closely related to σ is Heller's F parameter [43] which can be defined as

$$F = \sigma_{\min}/\sigma, \tag{22}$$

where $\sigma_{\min}$ is the dilution factor for all eigenstates under the feature envelope contributing with maximum intensity while preserving the width of the feature state. Due to quantum mechanical phase cancellation effects, F cannot exceed $1/3$. The nodal structure (orthogonality) of eigenstates prevents them from contributing maximally even in the global random matrix model. At long times, most molecules tend to obey this statistical measure, indicating that

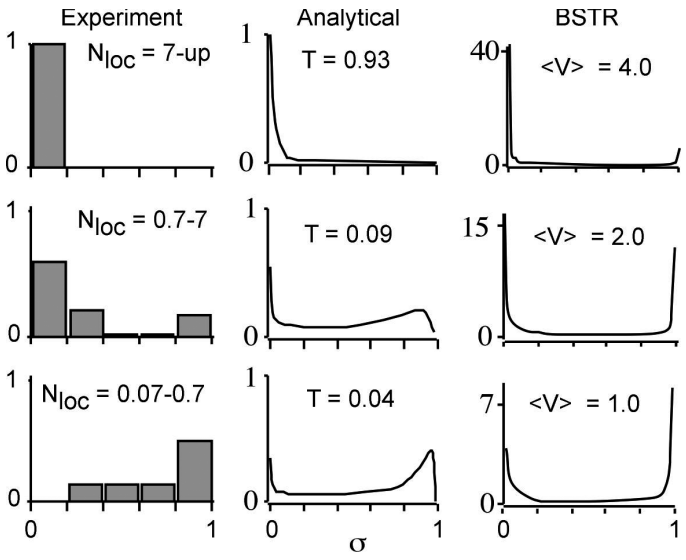

Figure 11. Experimental, analytical, and local random matrix model distribution functions of the dilution factor σ, or inverse number of participating states. Features break up into eigenstates, and this shows the distribution of the number of eigenstates per feature. The distributions are bimodal near the dephasing threshold, meaning that features either tend to break into many eigenstates, or are very robust against dephasing. $N_{\rm loc}$ is the local number of coupled states obtained by summing equation (14) over $n = 1$–4.

although equation (21) stems the dephasing process at intermediate times, state space is fully accessed as $t \to \infty$ once the energy threshold has been passed.

4.5. Hierarchical spectra

When a given initial state accesses only a small fraction of state space directly, and so does the next state, and so on, the resulting spectra will have a hierarchical structure. This is illustrated in figure 9, which shows experimental spectra for two molecules, $SCCl_2$ and methanol [38, 44]. In each case, the dephasing function $P(t)$ is shown in figure 10. Although the vibrational density matrix does eventually visit all of state space (i.e. the statistically predicted value of σ is reached) when the system is above the threshold, this happens with sub-exponential dynamics. Because couplings are local in state space, not necessarily small, slow dephasing also implies that the structure of the vibrational density matrix becomes randomized only gradually. This can be put on a firm mathematical footing by the quantity [12]

$$D(t) = 1 + \frac{[1 - \rho_{00}(t)]^2}{\mathrm{Tr}\{\mathrm{diag}[\rho_{ii}(t)]^2\} + \rho_{00}(t)^2}. \tag{23}$$

Here ρ_{00} is the component of the density matrix that corresponds to the feature state at $t = 0$. $D = 1$ at $t = 0$, and increases to $N_{\rm p}$, the number of participating states, as $t \to \infty$. On removing the initial state ρ_{00} from the trace, D counts how many states in addition to the initial state are participating in state space. In a GOE, D would immediately jump to $N_{\rm p}$ because states are globally connected, whereas in a locally coupled state space, D increases sub-exponentially towards $N_{\rm p}$ (figure 12).

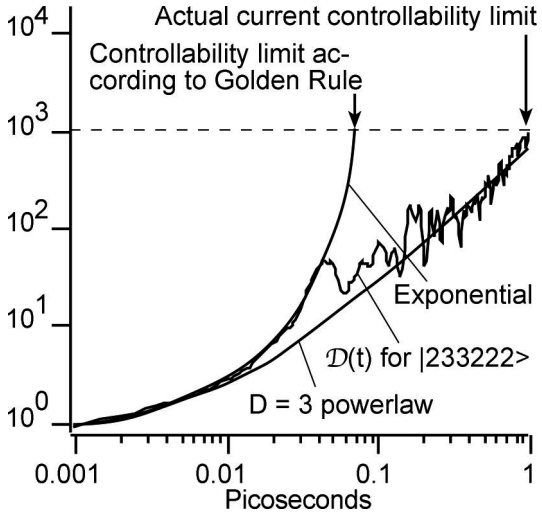

Figure 12. The number of state space cells $D(t)$ participating in dephasing of $SCCl_2$ increases as a power law with time. Because each cell requires an optical amplitude and phase for control, $2D(t)$ measures controllability. Current systems allow from 128 to 2000 degrees of freedom to be controlled. The time range for control is extended by over an order of magnitude compared to what is expected for a local random matrix model.

4.6. State space regularity and chemical reactions

Chemical reactions occur when the energy D is exceeded. At that point a bond is eventually broken and six vibrational modes are converted into three translational and three rotational modes (fewer if some fragments are linear). A particularly simple model treats the reaction as a decoherence mechanism on top of the internal dephasing of the system, by adding exponential decay terms $R(t)$ to the appropriate diagonal and off-diagonal matrix elements of the vibrational density matrix.

If the density matrix is represented in an eigenstate representation, then all states ρ_{ii} whose energy exceeds D will decohere; eigenstates of course will not dephase. In state space, the opposite is the case: all feature states will dephase, but reactivity is localized and only certain feature states will decohere. For example, to break an A–B bond, the A–B vibrational stretching mode must be excited to k quanta, so the mode energy exceeds D. Distributing the same energy into many modes does not produce a reactive state. Thus interior states are generally not reactive, while certain edge states in state space concentrate enough energy for reaction. The same type of argument applies to isomerization reactions where a bond is rotated to change the molecular shape because internal rotation modes scale similarly (section 2.3) [45].

Vibrational dephasing therefore affects reactivity in two ways. It can dephase an optically prepared reactive feature state, thereby potentially reducing the reaction rate; or it can dephase an unreactive feature state, thereby populating reactive feature states, usually via interior states. In the last case, dephasing makes the chemical reaction possible. Neither case implies that dephasing actually governs the reaction rate. If $P(t)$ decays much faster than $R(t)$, then the reaction rate will be determined by the ratio of the reactive states to the total number of energetically accessible cells in state space because the entire accessible phase space is populated by dephasing before the onset of decoherence [46]:

$$k \sim \frac{N_{\mathrm{R}}(\Delta E)}{\rho \Delta E}. \tag{24}$$

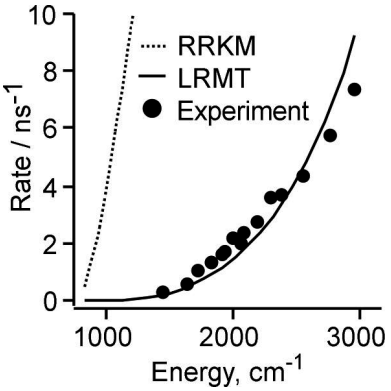

Figure 13. The molecule *trans*-stilbene (figure 1) isomerizes around the central carbon–carbon double bond with a barrier of about 1000 cm^{-1}. A local random matrix model given by Leitner and Wolynes, based on a potential surfaces computed by Martinez and co-workers, with dephasing parameters parametrized according to Bigwood and Gruebele obtains good agreement with experiment, while the global random matrix theory gives too fast a result. The reason is that slow dephasing restricts access to those states in state space which allow internal rotation about the double bond.

Here k is the rate, $N_R(\Delta E)$ is the number of reactive state space cells within an energy window ΔE, and ρ is the total density of states. This statistical limit includes RRKM theories for bond breaking (unimolecular reactions), and transition state theories for reactions involving collision and exchange of atoms (bimolecular reactions).

The timescales in practice are such that k varies from ns^{-1} to ps^{-1} as the energy increases from D to $1.1D$ above threshold, while the exponential deflationary phase of $P(t)$ lasts <0.1 ps when the excitation energy approaches D. For this reason, statistical formulae such as equation (24) generally provide a good description of reaction rates.

Slow dephasing, or the power law tail, can have an observable effect on reaction dynamics. If the tail extends significantly into the reaction timescale k^{-1}, the reaction rate is affected by dephasing: reactive edge states are populated more slowly than they decay, and the rate is decreased. Because $P(t)$ generally decays below 0.1–0.01 before the power law tail sets in, the effect will only cause a correction of a few per cent. If the initial dephasing is comparable to $R(t)$, the effect will be more pronounced. The best-studied experimental and computational example is the isomerization of *trans*-stilbene, which involves a rotation around the double bond in figure 1 [45, 47–51]. It occurs over a low barrier, so the energy scale D is comparable to $\hbar\omega$. Therefore dephasing is still near the threshold, and thus slow. Figure 13 shows experimental data for the isomerization rate of stilbene [52]. The statistical prediction has the rate increase as a function of energy much faster than the experimental observations. When vibrational dephasing is included using a model Hamiltonian of the form (8) based on frequencies ω_I and isomerization energies D from accurate electronic structure calculations, a slower reaction rate in agreement with experiment is obtained. In summary, the largest deviations from statistical theory would be expected in isomerization reactions with small D, although examples also exist for dissociation reactions.

5. Quantum control

Despite the power law tail, $P(t)$ decays rapidly enough for statistical theories to be a good approximation in most cases. Left to itself, dephasing would be an interesting curio that causes small corrections, usually less than a factor of two, in chemical reaction rates.

What makes slow dephasing interesting is that it opens up the possibility of optical quantum control [53]. Optical quantum control occurs when a molecule is continually subject to optical pulses that introduce additional couplings among states in state space [54–56]. These additional couplings can shape the vibrational density matrix, for example localizing it in a part of state space that gives rise only to a specific reaction product [9], or introducing entanglement that can be used for quantum computation [20]. If dephasing is fast, many states must be controlled; if dephasing is slow, only a small part of state space must be controlled, making control practically feasible. Each state in state space to be controlled optically requires one phase and one amplitude degree of freedom in the field. The controllability of the system is thus determined by $2D$ from equation (23) [9]. Currently, pulse shaping of femtosecond pulses limits the number of degrees of freedom to <2000, and no exponential growth in this technology can be expected. Thus, it makes an important difference whether the number N of cells in state space required to describe the vibrational density matrix grows as a polynomial instead of as an exponential function of time. Control is feasible over a much longer period of time (figure 12) in the former case.

This is illustrated in figure 14 for a particular type of quantum control: 'freezing' an initially prepared feature state that would normally undergo dephasing [9]. This is not the most general type of quantum control possible on a feature state, but it has several desirable properties, and we use it as an example throughout. Firstly, the initially prepared state may have symmetry properties that cause it to react to form specific products, while the full set of states accessed statistically produce a number of reaction products. Secondly, freezing a vibrational feature has the advantage that only the local structure of state space around the feature needs to be known. This information is generally available if the feature can be accessed optically. The idea behind quantum control then is to adjust the amplitude and phase degrees of freedom of the field in order to 'freeze', or stabilize, a feature state and prevent it from dephasing.

In the following subsections the quantum–classical and second-quantized theory for optical control of vibrational dephasing will be described briefly. Finally, the utility of molecular vibrational modes for modelling quantum computers with a small number of qubits will be discussed.

5.1. Quantum–classical control

In this approach, the vibrational degrees of freedom are treated quantum mechanically, while the molecule–field interaction is treated classically [57]:

$$H(t) = K + V - \hat{\mu} E(\mathbf{c}, t), \tag{25}$$

where K is the molecular kinetic energy operator, V is from equations (4) or (8), $\hat{\mu}$ is the transition dipole operator discussed in 3.2, and $E(\mathbf{c}, t)$ is the classical electric field with adjustable amplitude and phase parameters $\mathbf{c}$. Many representations of the electric field are possible. A particularly useful one expands the field in wavelets [9]. At each field frequency, a pair of wavelets describes the amplitude and phase of the field. This allows optimization algorithms to operate simultaneously on the coarse-grained and fine-grained features of the electric field.

An extensive methodology for optimizing the field, subject to constraints on the wavefunction and field, has been developed by Rabitz and co-workers based on optimal control concepts from engineering [58, 59]. Formal analyses of the controllability of quantum systems by classical fields have been developed [60]. The goal is to treat the system as much as possible as a 'black box' to facilitate optimization in the absence of experimental knowledge. The

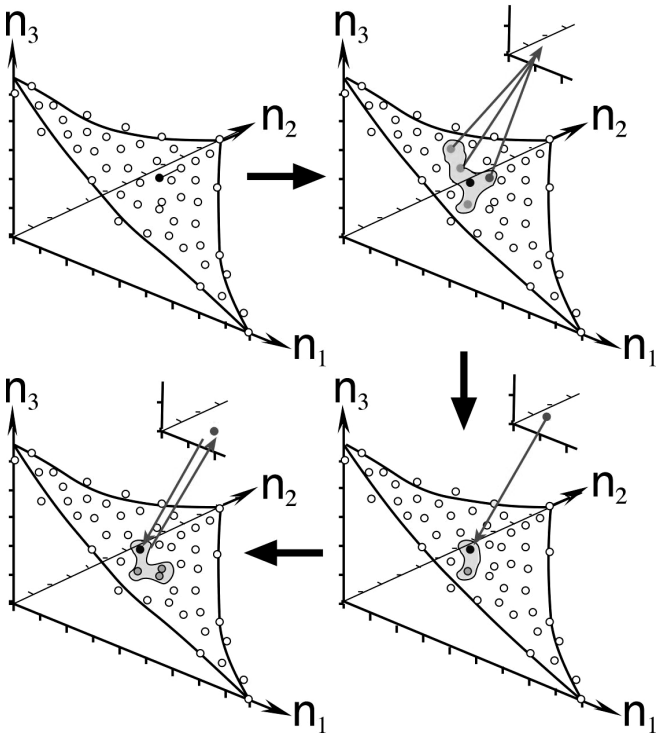

Figure 14. Quantum control to 'freeze' a wavepacket. An initially prepared feature (upper left panel) begins to dephase (upper right panel). Its undesirable components are cycled to a different set of vibrational/electronic states by a shaped, phase-coherent laser pulse (upper right panel), then returned to the desired feature by another shaped pulse (lower right panel). This cycle is repeated to keep the feature 'frozen,' although in practice leakage occurs because the optical field cannot cycle all necessary quantum states with 100% efficiency (lower left panel). This corresponds to the controllability limit in figure 12. 'Freezing' is more robust than more general 'guiding' of wavepackets by quantum control because it requires only two local domains of state space, which are both optically accessible and whose structure/Hamiltonian is therefore known.

optimization target functional has the general form

$$T(\mathbf{c}) \sim \int_{-\infty}^{\infty} \mathrm{d}t\; W(t)\, \mathrm{Tr}\left\{ \rho_{\mathrm{Target}}\; O_t \mathrm{e}^{-\mathrm{i}\int H(\mathbf{c},t)\mathrm{d}t}\, \rho_0\, \mathrm{e}^{+\mathrm{i}\int H(\mathbf{c},t)\mathrm{d}t} \right\}. \tag{26}$$

In this equation, the initial density matrix is propagated in time and overlapped with the target density matrix. This overlap is to be maximized in a time window $W(t)$ by adjusting $\mathbf{c}$. (The ordering operator O_t is required because H is time dependent.) Equation (26) requires nonlinear optimization.

Here we pursue a more explicit path, motivated by the observation that the vibrational couplings subject to control are local in state space, thus making the control more robust than would be anticipated for a global random matrix Hamiltonian. We lift off the black box and use the simplifying properties of the control Hamiltonian. A particularly favourable representation of the dynamics uses a wavelet expansion of the electric field, and uses the SUR algorithm to compute the dynamics of the vibrational density matrix [9, 61]. Simulated annealing or a genetic algorithm then maximizes the overlap of the time-evolving vibrational state with the initial feature state, thus 'freezing' the wavepacket. The applied electric field effectively cancels out the vibrational couplings that lead to dephasing.

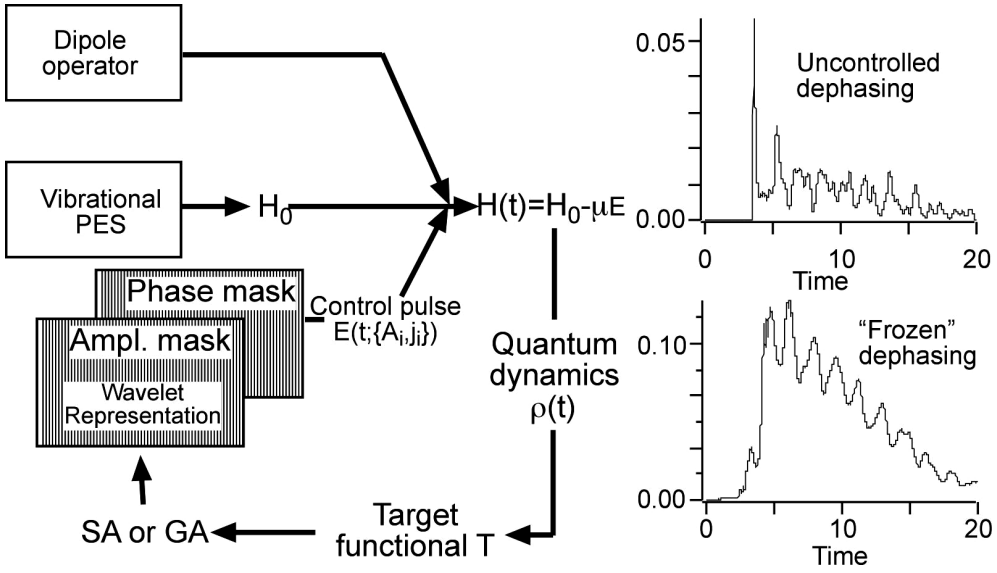

Figure 15. Quantum control for 'freezing' a wavepacket using the quantum–classical formalism. The wavefunction is propagated in time using the Hamiltonian, and the target functional is computed. Guesses at improved optical field degrees of freedom are generated using simulated annealing (SA) or genetic algorithms (GA), to simulate the phase and amplitude control masks of an experiment. Wavelets represent the phases and amplitudes hierarchically, to match the hierarchical structure of the spectra. On the left, uncontrolled dephasing and 'frozen' dephasing are shown. Because the optical field controls a finite number of degrees of freedom, freezing is achieved for a finite duration (see figure 14).

In terms of the eigenstate picture for a pure system, the dynamics appears rather trivial: the phases of the eigenstates evolve at different rates, and the applied electric field cycles each eigenstate phase coherently to another state and back, with the correct phase lag to cancel out the time evolution, thus preserving the initial state. However, if a large molecule were described by a global random matrix, control would be practically impossible at energies $\sim D$ because the number of eigenstates would greatly exceed the number of control parameters **c**. This is where hierarchical dephasing comes to the rescue: the number of states in state space required to describe the vibrational density matrix increases only geometrically in time, not exponentially. In state space, quantum control can be pictured as in figure 14: a localized feature is initially prepared. It slowly leaks to nearby states, which are cycled back with the correct phase to the original feature by the electric field. A small number of degrees of freedom **c** are required as long as the density matrix remains localized. Of course, the control is not perfect and eventually the vibrational density matrix will leak into undesirable portions of state space.

The quantum–classical control scheme and a calculation showing 'freezing' of vibrational dephasing in $SCCl_2$ for a limited but useful period of time are shown in figure 15. The 10 ps timescale achieved is useful because reaction rates are of the order of ps^{-1} above the threshold D, so dephasing can no longer randomize the vibrational density matrix, thereby making nonstatistical outcomes possible.

5.2. Fully quantum control

The external field can also be quantized, replacing equation (25) by

$$H = K + V + \sum \hbar\omega_k (a_k^\dagger a_k + \tfrac{1}{2}) + \sum c_k [K + V, \hat{\mu}](a_k^\dagger + a_k). \tag{27}$$

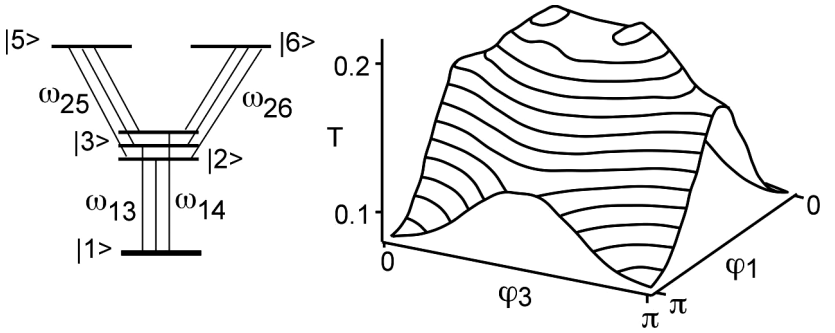

Figure 16. The full quantum control calculation for a six-level system with initial density matrix $|1\rangle\langle 1|$, three intermediate states, and two 'product' states $|5\rangle$ and $|6\rangle$. The allowed transitions are shown as lines. Equation (29) is computed using the known energy level spacings and transition dipole moments, with either a path integral representation for the harmonic field degrees of freedom, or a filtered basis set containing coherent field states $|\bar{n}, \varphi\rangle$ parametrized by amplitude and phase and six molecular states. A 2D cut though the full phase/amplitude control surface is shown, showing symmetry relations between two of the phases.

For simplicity, polarization degrees of freedom are not included. At a first glance, equation (27) appears as a major complication over equation (25) because a classical parametric electric field has been replaced by an infinite number of quantum degrees of freedom. In practice, the situation is not as bad because the harmonic oscillator representation is exact for photons, and path integral and other efficient solution methods exist for a bath of harmonic oscillators coupled linearly to a system. Equation (27) introduces another important advantage over equation (25). The control functional now becomes

$$T(\mathbf{c}) \sim \int_{-\infty}^{\infty} \mathrm{d}t\; W(t)\, \mathrm{Tr}\left\{ \rho_{\mathrm{Target}}\, \mathrm{e}^{-\mathrm{i}tH/\hbar}\, \rho_0(\mathbf{c})\, \mathrm{e}^{+\mathrm{i}tH/\hbar} \right\}. \tag{28}$$

The dependence on the control parameters no longer occurs in the exponential because the full Hamiltonian (27) is nonparametric. Thus powerful tools of linear optimization can be brought to bear on the problem. The integral in equation (28) has been evaluated explicitly [62]:

$$T[\mathbf{c}] \sim \sum_i (\rho_T(\mathbf{c}))_{ii} (\rho_0(\mathbf{c}))_{ii} \tag{29}$$

and $T[\mathbf{c}]$ obtained noniteratively by using the Hellmann–Feynman theorem (only matrix elements of the density operators connecting states of equal energy appear in equation (29)) and single-step linear optimization.

Figure 16 applies the methodology to a simple model system useful in quantum control of chemical reactions. The density matrix is initially in the ground state, and coherent interaction with photons via a set of intermediate states can be used to optimize population of either a 'left' or 'right' product state. A two-dimensional cut through the optimization surface as a function of two phase angles is shown. To provide well-defined phase angles, a coherent state basis for the field is used to evaluate equation (29), rather than a number state basis. Figure 16 also illustrates a useful approximation that can be made to describe the field, and which is already implicit in equation (27): the bound part of the potential V supports a discrete set of states, and in the continuum the two 'product' states must be isoenergetic so quantum control is possible as $t \to \infty$. Therefore only a discrete set of frequencies are required to represent the field, and if a finite number of field cycles of the type shown in figure 15 are sufficient, a rather small set of oscillators are required in equation (27).

Full molecular quantum control opens up the possibility of more information-rich molecular spectroscopies. When a quantum–classical Hamiltonian is used to describe molecule–field interactions, the emphasis is on how the field controls the molecule. The situation is more symmetrical in equation (27). Interaction with the molecule modifies the phases and amplitudes of the field degrees of freedom. Of course molecular spectroscopy is as old as the study of molecules, and single-photon techniques such as absorption or emission spectroscopy, and multi-photon techniques such as the one needed to effect control in figure 14, have undergone decades of development. Yet equation (28) indicates the possibility of novel linear and nonlinear spectroscopies based on quantum control. The target density matrix contains information about field degrees of freedom beyond the overall intensity of the field as a function of wavelength or wavevector. Even a simple linear absorption process can create complex field patterns, which can be detected with amplitude- and phase-sensitive detectors. Thus much more information can be extracted about the state of a molecule by studying degrees of freedom of the output field beyond overall intensity or average wavevector. This will require a new generation of detectors that can monitor phase and amplitude of output fields as a function of time and position, but prototypes of such detectors have already been reported [63].

5.3. Optical molecular quantum computing

The Hamiltonian in equations (3) and (4) has another potential application: few-qubit quantum computing. Quantum computation requires a source of qubits (two-level systems), and methods for entangling them as well as for performing measurements on them. The biggest problem currently faced by even small model systems for quantum computers is the purity of states [64]. The decoherence of candidate systems is often very fast, and electromagnetic radiation creates only very small deviations from a diagonal density matrix. NMR models for quantum computing are an example of the problems faced: although individual molecules may reach a large degree of coherence, they cannot be probed individually because of the low sensitivity associated with magnetic dipole transitions, and the whole ensemble is nearly diagonal [19, 65]. This can be circumvented by picking systems whose characteristic energy scale D greatly exceeds kT, such as optically trapped ions [66]. Such systems still suffer from slow time evolution because of the constraints of transferring coherence among the qubits.

Molecular vibrations provide a convenient system for few-qubit quantum computing: the energy scale ω to D at which states are excited can be set to greatly exceed kT, so pure states can be created to a good approximation optically; mode couplings and phase-coherent optical transfer of amplitude can create entangled states on a femtosecond timescale and modify their phases; nonthermal decoherence mechanisms such as fluorescence are slow by comparison to the computing process (nanosecond versus sub-picosecond); larger molecules can serve as their own 'baths,' allowing the effects of dephasing (decoherence in a reduced density matrix) to be studied in detail, and with a great degree of experimental control, as described above.

One way of implementing qubits and operations on qubits by using quantum control of molecular vibrations has been discussed in [20]. In this approach, each vibrational degree of freedom in state space can be used to represent one qubit, for a total of N qubits in an N-oscillator molecule. In principle, quite respectable numbers of qubits can be achieved; for example, $N = 84$ qubits could be implemented in a molecule such as cyclohexylaniline in figure 1. In practice, the number of qubits is limited to the modes separately addressable via infrared optical excitation. Figure 6 illustrates how a 3D molecular state space could implement two qubits via two accessible modes. Each mode is of course an anharmonic oscillator and not a two-level system, but anharmonicity is often large enough (>2 meV or 1 ps timescale) that fast optical pulse sequences can address only the lowest two states without too much unwanted

leakage into higher energy states. Thus the weak anharmonicity of the molecular system can mimic the very strong effective anharmonicity of a two-level system [20].

Implementing a Hadamard transform

$$\mathrm{HA} = \begin{pmatrix} 1 & 1 \\ 1 & -1 \end{pmatrix} \tag{30}$$

on a single mode requires a pulse sequence that will put the mode in a superposition state of its ground and first excited vibrational levels, without affecting any of the other modes. This has been demonstrated computationally with >98% efficiency because ω_I is sufficiently different for different molecular modes that they are individually optically addressable. The individual addressability of low energy interior states in state space also allows entangled states to be prepared optically, such as by pumping $|00\rangle \rightarrow (|00\rangle \pm |11\rangle)/\sqrt{2}$. Phase shift operations can be effected in the simplest case by free propagation (e.g. the two $\pm$ states in the previous sentence interconvert on a timescale $\pi/[\omega_1 + \omega_2]$). However, universal phase shift pulses in the presence of multiple qubits are more difficult to realize because multiple states evolve with different phases. Qubits can interact via low order mode couplings such as the local mode coupling $q_1 q_2$, which mixes the $|01\rangle$ and $|10\rangle$ local mode states. Efficiencies in the 70% range or higher have been computed for various types of logic gate using the molecule acetylene, so dephasing effects that reduce the perfection of quantum logic gates can be kept small [20]. Decoherence is negligible in molecular beams, where infrared emission lifetimes, interaction lifetimes, and collision lifetimes lie in the microsecond range, about 10^9 times slower than the computational process.

The vibrational Hamiltonian can also be exploited for quantum computing in a different way. As discussed in section 4, state space is accessed locally by optical excitation (local dipole operator), and dephasing processes are local (equation (4)). Quantum control with a reasonable number of control parameters can thus be used to implement quantum logic gates in highly vibrationally excited molecules. Rather than mapping each qubit onto a single mode, one can make use of the equivalence of a system with $m = 2^N$ nondegenerate states, whose phases and amplitudes can be arbitrarily adjusted by optical pulses, with an N-qubit system [67].

In order to compute with qubits in this form, one has to effect arbitrary unitary transformations among the 2^N states. If the m states being manipulated are approximately vibrational eigenstates, such manipulations can be done by combining free evolution (introducing phase shifts) and population transfers via a gateway state $|g\rangle$ (amplitude and phase changes). The latter is done by resonantly pumping from a state $|m_i\rangle$ to $|g\rangle$, then from $|g\rangle$ to $|m_j\rangle$, and repeating this cycle with other pairs of states until the desired phase/amplitude transformation has been accomplished on the set of states $\{|m_i\rangle\}$. The individual cycles in such a scheme have been called 'STIRAP' [55]. The implementation of such pulse sequences to perform gate operations is more complicated than in the 'one mode per qubit' approach because individual qubits no longer can be addressed by a single wavelength (for example, the energy difference between states $|00\rangle$ and $|01\rangle$ no longer even approximately equals the energy difference between $|10\rangle$ and $|11\rangle$ states, so the second qubit cannot be individually addressed by a single colour). Thus full wavelength multiplexing is required, which makes the addressing of the N-qubit system grow as 2^N. This is a general problem faced by quantum computing schemes: even if the computation is very efficient, the process of encoding (or decoding) the information may be exponentially complex.

Figure 9 illustrates an energy range of 37 meV in the spectrum of $SCCl_2$ that contains 32 optically addressable feature states, sufficient to implement five qubits. Quantum control for the same energy range is demonstrated in figure 15. The dynamical range of timescales is thus $2\pi/37$ meV $\sim$ 0.1 ps to $2\pi/32/37$ meV $\sim$ 3 ps. The 32 features undergo dephasing in

state space that is fully controllable on a 10 ps timescale (figure 15), so gate operations can be completed on the 3 ps timescale required. Although molecular vibrations are not scalable to large numbers of qubits, they present us with a useful atomic-scale laboratory with controllable effects of dephasing on quantum logic gates.

6. Solvent–molecule interaction and decoherence

So far, we have mainly considered molecules as their own 'heat baths'. If the entire density matrix is examined, only dephasing is possible and the purity of the initial vibrational density matrix is maintained. Yet as shown in figure 2, even a very small molecule with only six degrees of freedom can be discussed using the language of reduced density matrices. Each mode of $SCCl_2$ is decohered by the ensemble of the remaining five modes, and its population approaches a Bose–Einstein distribution via a power law decay. Molecular vibrations thus provide a nice model system for discussing the connection between dephasing and decoherence.

The decoherence of molecular vibrations by an external solvent is also of great interest [68–72]. For some molecules, it can be surprisingly slow. For example, it comes as no surprise that in the gas phase, the dissociation of an HgI_2 (mercury iodide) molecule produces products whose vibrational motions are coherently locked to the initial vibrational motion resulting from the dissociation process [73]. Analogous experiments in the condensed phase have shown that phase coherence is maintained for a period of several vibrations when the same reaction is examined in a weakly coupling solvent [68]. Nonetheless, statistical models predicting Lorentzian lineshapes generally provide a satisfactory description of decoherence, and line broadening models such as Brownian oscillators coupled to the system are used successfully to describe the dynamics [74].

Here we discuss a different kind of toy model, based on the Caldeira–Leggett Hamiltonian [75], which differentiates dynamics caused by different solvent shells [18]. Figure 17 illustrates the model. Rather than describing the solute molecule in great detail, and treating the solvent like a set of harmonic oscillators linearly coupled to the solute but not to one another (see equation (27)), we treat the solute like a two-level system, but include the shell structure of the solvent, and anharmonic couplings within and among solvent shells:

$$H = \frac{hc\Delta}{2}\sigma_z + \frac{hc\Delta}{2}\sigma_x + \sum V_i(a_i^\dagger + a_i) + \sum \hbar\omega_i\left(a_i^\dagger a_i + \frac{1}{2}\right) + \sum_{n=3}\sum_{[n_i]}(\pm 1)\prod_{i=1}^{N} c_i^{n_i}(a_i^\dagger + a_i)^{n_i}. \tag{31}$$

In equation (29), $\sigma_{x,y}$ are Pauli matrices, Δ is the tunnelling splitting, and V_i is a coupling of the two-level system to the first shell of bath modes. The ω_I are the solvent frequencies contributing to the spectral density, and the c_i are couplings within and among bath shells, such that the first shell couples only to the second, the second to the first and third, etc. When enough shells are included, the quasi-continuous but structured spectral density shown in figure 17 is obtained. The model chooses to examine in more detail the dynamics within the solvent, and not the solute. It goes beyond the linear response approximation so the coupling parameters are not temperature dependent (as they have to be if the spectral density is modelled by a set of uncoupled harmonic oscillators).

The results in figure 17 show that the decoherence of the two-level system by the solvent degrees of freedom can be polynomial in time rather than exponentially fast with realistic choices of the coupling constants. In this model, increasing the density of states by adding more harmonic degrees of freedom to the first shell or by increasing the number of shells, or

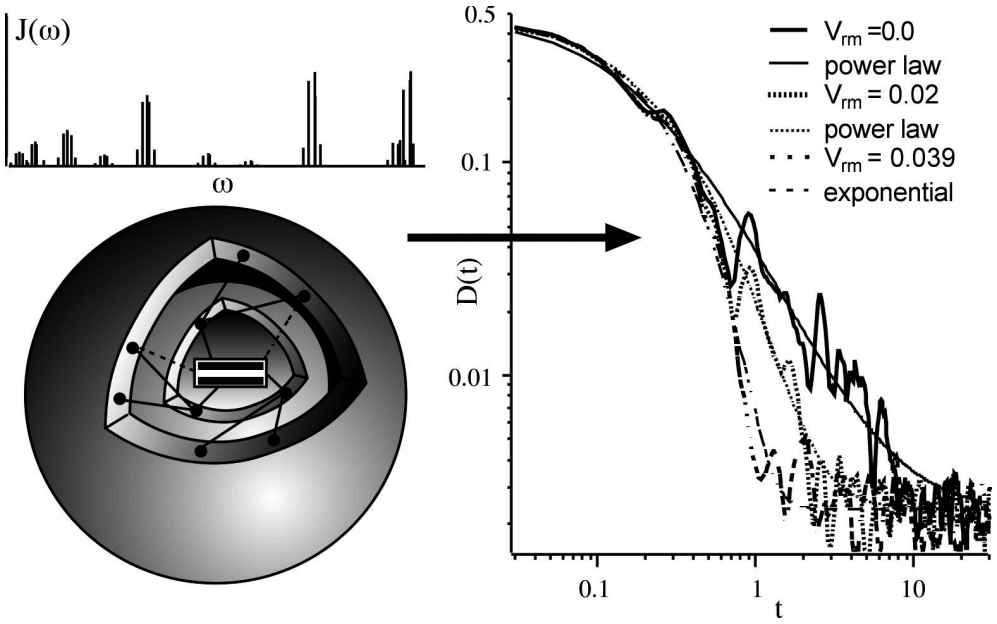

Figure 17. The toy model for interaction of solvent shells with a two-level solute. The greater the number of shells added, the closer the approach of the spectral density $J(\omega)$ to a continuous function. On the right the decoherence of the TLS according to equation (32) is computed for different intrabath coupling strengths (relative to the TLS splitting). Intrabath couplings, not a continuous spectral density or large system–bath couplings, are the most efficient mechanism for obtaining exponential decoherence as opposed to a power law.

by increasing the strength of the couplings between the bath and two-level system, are not the most efficient means of wiping out sub-exponential decoherence. Increasing the anharmonic couplings among first-shell degrees of freedom, and to a lesser extent increasing anharmonic couplings to the second shell proved most effective at inducing exponentially fast decoherence of the two-level system, as monitored by the magnitude of the off-diagonal matrix element of the reduced two-level system density matrix,

$$D(t) = |\langle +| \operatorname{Tr}_{\mathrm{Bath}}\{\rho(t)\}|-\rangle|^2. \tag{32}$$

Anharmonic couplings within the bath, and exchange of degrees of freedom between the first and higher shells are thus the most effective means of introducing decoherence when the bath is discrete. Although a number of beautiful results have been obtained for the strict spin-boson Hamiltonian with a purely harmonic continuous bath, equation (31) is probably a more accurate model for real molecule–solvent interactions: solvation shells exist in real solvents (typically 4–10 molecules in the first shell), and have a limited number of degrees of freedom. Thus even for interactions with a solvent, a local density of states rather than a global density of states is important, and it is strong couplings among states comprising the local density of states that give rise to exponential dephasing. In that case, decoherence in a weakly coupled solvent will ultimately be limited by diffusion of degrees of freedom from one shell to another, a process that usually occurs on a timescale of picoseconds, thus potentially leaving a window for quantum control of the solute even in a condensed phase environment.

Acknowledgment

This work was supported by the National Science Foundation.

References

[1] Monroe C, Meekhof D M, King B E and Wineland D J 1996 A 'Schrödinger cat' superposition state of an atom *Science* **272** 1131
[2] Feurer T, Vaughan J C and Nelson K A 2003 Spatiotemporal coherent control of lattice vibrational waves *Science* **299** 374
[3] Bardeen C J, Che J, Wilson K R, Yakovlev V V, Apkarian V A, Martens C C, Zadoyan R, Kohler B and Messina M 1997 Quantum control of I_2 in the gas phase and in condensed phase solid Kr matrix *J. Chem. Phys.* **106** 8486
[4] Gutzwiller M C 1990 *Chaos in Classical and Quantum Mechanics* (New York: Springer)
[5] Robnik M 1994 Recent developments in energy level statistics in generic systems between integrability and chaos *Prog. Theor. Phys.* (Suppl. 116) 331
[6] Gruebele M 1996 Bose statistics triangle rule model for intramolecular vibrational energy redistribution *J. Phys. Chem.* **100** 12183
[7] Pearson B J, White J L, Weinacht T C and Bucksbaum P H 2001 Coherent control using adaptive learning algorithms *Phys. Rev.* A **63** 063412
[8] Brixner T and Gerber G 2003 Quantum control of gas-phase and liquid-phase femtochemistry *Chem. Phys. Chem.* **4** 418
[9] Bigwood R M and Gruebele M 2002 Freezing molecular vibrational energy flow with coherent control *J. Mol. Struct. (Theochem)* **589** 447
[10] Logan D E and Wolynes P G 1990 Quantum localization and energy flow in many-dimensional Fermi resonant systems *J. Chem. Phys.* **93** 4994
[11] Bigwood R and Gruebele M 1995 A simple matrix model of intramolecular vibrational redistribution and its implications *Chem. Phys. Lett.* **235** 604
[12] Wong V and Gruebele M 1999 How does vibrational energy flow fill the molecular state space? *J. Phys. Chem.* **103** 10083
[13] Oka T 1967 Vibration–rotation interaction in symmetric-top molecules and the splitting between A1 and A2 levels *J. Chem. Phys.* **47** 5410
[14] Madsen D, Pearman R and Gruebele M 1997 Approximate factorization of molecular potential surfaces. I. Basic approach *J. Chem. Phys.* **106** 5874
[15] Pearman R and Gruebele M 1998 On the importance of higher order anharmonic molecular couplings *J. Chem. Phys.* **108** 6561
[16] Schofield S and Wolynes P G 1993 A scaling perspective on quantum energy flow in molecules *J. Chem. Phys.* **98** 1123
[17] Gruebele M 1998 Intramolecular vibrational dephasing obeys a power law at intermediate times *Proc. Natl Acad. Sci. USA* **95** 5965
[18] Wong V and Gruebele M 2002 Sub-exponential spin-boson decoherence in a finite bath *Chem. Phys.* **284** 29
[19] Vandersypen L M K, Steffen M, Breyta G, Yannoni C S, Cleve R and Chuang I L 2000 Experimental realization of an order-finding algorithm with an nmr quantum computer *Phys. Rev. Lett.* **85** 5452–5
[20] Tesch C M, Kurtz L and Vivie-Riedle R D 2001 Applying optimal control theory for elements of quantum computation in molecular systems *Chem. Phys. Lett.* **343** 633
[21] Papousek D and Aliev M R 1982 *Molecular Vibrational–Rotational Spectra* (Amsterdam: Elsevier)
[22] Bullock W J, Adams D K and Lawrance W D 1990 Calculations of vibrational state mixing leading to intramolecular vibrational relaxation in S_1 anthracene: comparison with quantum beat experiments *J. Chem. Phys.* **93** 3085
[23] Pearman R and Gruebele M 2000 Approximate factorization of molecular potential surfaces II. Internal rotors *Z. Phys. Chem.* **214** 1439
[24] Strickler B and Gruebele M 2004 Vibrational state structure of $SCCl_2$ from the zero point to the first dissociation limit *Phys. Chem. Chem. Phys.*
[25] Wong V and Gruebele M 2001 Nonexponential dephasing in a local random matrix model *Phys. Rev.* A **63** 22502
[26] Leitner D M and Wolynes P G 1996 Many-dimensional quantum energy flow at low energy *Phys. Rev. Lett.* **76** 216

[27] Schofield S A and Wolynes P G 1995 Rate theory and quantum energy flow in molecules: modeling the effects of anisotropic diffusion and dephasing *J. Phys. Chem.* **99** 2753
[28] Gambogi J E, Timmermans J H, Lehmann K K and Scoles G 1993 Enhanced instability of extreme motion states in propyne: lifetimes of overtone versus isoenergetic combination states *J. Chem. Phys.* **99** 9314
[29] Nesbitt D J and Field R W 1996 Vibrational energy flow in highly excited molecules–role of intramolecular vibrational redistribution *J. Phys. Chem.* **100** 12735
[30] Silva M, Jongma R, Field R W and Wodtke a M 2001 The dynamics of stretched molecules: experimental studies of highly vibrationally excited molecules with stimulated emission pumping *Annu. Rev. Phys. Chem.* **52** 811
[31] Keske J C and Pate B H 2000 Decoding the dynamical information embedded in highly mixed quantum states *Annu. Rev. Phys. Chem.* **51** 323
[32] Stuchebrukhov a A, Kuzmin M V, Bagratashvili V N and Lethokov V S 1986 Threshold energy dependence of IVR in polyatomic molecules *Chem. Phys.* **107** 429
[33] Stuchebrukhov a A, Mehta A and Marcus R A 1993 Vibrational superexchange mechanism of intramolecular vibrational relaxation in $(CH_3)_3CCCH$ *J. Phys. Chem.* **97** 12491
[34] Heller E J 1995 Dynamical tunneling and molecular spectra *J. Phys. Chem.* **99** 2625
[35] Callegari A, Pearman R, Choi S, Engels P, Srivastava H, Gruebele M, Lehmann K K and Scoles G 2002 Intramolecular vibrational relaxation in aromatic molecules II. An experimental and computational study of pyrrole and triazine near the IVR threshold *Mol. Phys.* **101** 551
[36] Uzer T 1991 Theories of intramolecular vibrational energy transfer *Phys. Rep.* **199** 73
[37] Schofield S A, Wyatt R E and Wolynes P G 1995 Computational study of many-dimensional quantum energy flow: from action diffusion to localization *Phys. Rev. Lett.* **74** 3720–3
[38] Boyarkin O V, Rizzo T R and Perry D S 1999 Intramolecular energy transfer in highly vibrationally excited methanol. II. Multiple timescales of energy redistribution *J. Chem. Phys.* **110** 11346
[39] Smith P G and McDonald J D 1990 Picosecond fluorescence depletion spectroscopy. III. Intramolecular vibrational relaxation in the excited electronic state of p-cyclohexylaniline *J. Chem. Phys.* **92** 1004
[40] Bigwood R and Gruebele M 1997 Models of intramolecular energy redistribution spanning deterministic and statistical approaches *ACH Models Chem.* **134** 675
[41] Bigwood R, Gruebele M, Leitner D M and Wolynes P G 1998 The vibrational energy flow transition in organic molecules: theory meets experiment *Proc. Natl Acad. Sci. USA* **95** 5960
[42] Leitner D M and Wolynes P G 1996 Statistical properties of localized vibrational eigenstates *Chem. Phys. Lett.* **258** 18
[43] Stechel E B and Heller E J 1984 Quantum ergodicity and spectral chaos *Annu. Rev. Phys. Chem.* **35** 563
[44] Bigwood R, Milam B and Gruebele M 1998 The ground state vibrational structure of $SCCl_2$: experimental observation of on-resonant energy flow *Chem. Phys. Lett.* **287** 333
[45] Leitner D M and Wolynes P G 1997 Quantum energy flow during molecular isomerization *Chem. Phys. Lett.* **280** 411
[46] Marcus R A 1952 Unimolecular dissociations and free radical recombination reactions *J. Chem. Phys.* **20** 359
[47] Lee M, Holtom G R and Hochstrasser R M 1985 Observation of the Kramers turnover region in the isomerism of trans-stilbene in fluid ethane *Chem. Phys. Lett.* **118** 359
[48] Courtney S H, Balk M W, Philips L A and Fleming G R 1988 Unimolecular reactions in isolated and collisional systems—deuterium isotope effect in the photoisomerization of stilbene *J. Chem. Phys.* **89** 6697
[49] Nordholm S 1989 Photoisomerization of stilbene—a theoretical study of deuteration shifts and limited internal vibrational redistribution *Chem. Phys.* **137** 109
[50] Baskin J S, Bañares L, Pedersen S and Zewail a H 1996 Fs real-time probing of reactions. 20. Dynamics of twisting, alignment, and IVR in the trans-stilbene isomerization reaction *J. Phys. Chem.* **100** 11920
[51] Leitner D M, Levine B, Quenneville J, Martinez T J and Wolynes P G 2003 Quantum energy flow and trans stilbene photoisomerization: an example of a non-RRKM reaction *J. Phys. Chem.* A **107** 10706–16
[52] Felker P M, Lambert W R and Zewail a H 1985 Dynamics of intramolecular vibrational-energy redistribution (IVR). IV. Excess energy dependence, t-stilbene *J. Chem. Phys.* **82** 3003
[53] Gruebele M and Bigwood R 1998 Molecular vibrational energy flow: beyond the golden rule *Int. Rev. Phys. Chem.* **17** 91
[54] Tannor D J and Rice S A 1985 Control of selectivity of chemical reaction via control of wavepacket evolution *J. Chem. Phys.* **83** 5013
[55] Rice S A and Zhao M 2000 *Optical Control of Molecular Dynamics* (New York: Wiley)
[56] Shapiro M and Brumer P 1986 Laser control of product quantum state populations in unimolecular reactions *J. Chem. Phys.* **84** 4103

[57] Shi S, Woody A and Rabitz H 1988 Optimal control of selective vibrational excitation in harmonic linear chain molecules *J. Chem. Phys.* **88** 6870
[58] Warren W S, Rabitz H S and Dahleh M 1993 Coherent control of quantum dynamics: the dream is alive *Science* **259** 1581
[59] Rabitz H and Zhu W S 2000 Optimal control of molecular motion: design, implementation, and inversion *Acc. Chem. Res.* **33** 572
[60] Clark a W, Lucarelli D G and Tam T J 2003 Control of quantum systems *Int. J. Mod. Phys.* B **17** 5397
[61] Bigwood R and Gruebele M 1995 Shifted-update rotation: simple integration of the many-level Schrödinger equation to long times *Chem. Phys. Lett.* **233** 383
[62] Gruebele M 2001 Fully quantum coherent control *Chem. Phys.* **267** 33
[63] Marks D L, Stack R A and Brady D J 1999 Three-dimensional coherence imaging in the Fresnel domain *Appl. Opt.* **38** 1332
[64] Wu L-A and Lidar D A 2002 Creating decoherence-free subspaces using strong and fast pulses *Phys. Rev. Lett.* **88** 207902
[65] Braunstein S L, Caves C M, Jozsa R, Linden N, Popescu S and Schack R 1999 Separability of very noisy mixed states and implications for NMR quantum computing *Phys. Rev. Lett.* **83** 1054
[66] Lucas D M, Donald C J S, Home J P, McDonnell M J, Ramos A, Stacey D N, Stacey J P, Steane a M and Wester S C 2003 Oxford ion-trap quantum computing project *Phil. Trans. R. Soc.* A **361** 1401
[67] Weidinger D and Gruebele M 2004 Mapping n qubits into an ensemble of 2^n vibrational states, in preparation
[68] Owrutsky J C, Raftery D and Hochstrasser R M 1994 Vibrational relaxation dynamics in solution *Annu. Rev. Phys. Chem.* **45** 519
[69] Courtney S H and Fleming G R 1985 Photoisomerization of stilbene in low viscosity solvents—comparison of isolated and solvated molecules *J. Chem. Phys.* **83** 215
[70] Deak J C, Iwaki L K and Dlott D D 1999 Vibrational energy redistribution in polyatomic liquids: ultrafast IR–Raman spectroscopy of acetonitrile *J. Phys. Chem.* **102** 8193
[71] Laenen R, Rauscher C and Laubereau A 1998 Vibrational energy redistribution of ethanol oligomers and dissociation of hydrogen bonds after ultrafast infrared excitation *Chem. Phys. Lett.* **283** 7
[72] Heckscher M M, Sheps L, Bingemann D and Crim F F 2002 Relaxation of the C–H stretching fundamental vibrations of CHI3, CH2I2, and CH3I in solution *J. Chem. Phys.* **117** 8917
[73] Gruebele M, Roberts G and Zewail a H 1990 Femtochemistry of the reaction of IHgI: theory versus experiment *Phil. Trans. R. Soc.* A **332** 223
[74] Tuckerman M and Berne B J 1993 Vibrational relaxation in simple fluids: comparison of theory and simulation *J. Chem. Phys.* **98** 7301
[75] Caldeira a O and Leggett a J 1983 Quantum tunneling in a dissipative system *Ann. Phys.* **149** 374
[76] Gruebele M and Wolynes P 2004 Vibrational energy flow and chemical reactions *Acc. Chem. Res.* **37** 261